

Fall 2003

Vibration Analysis of a Fan/Compressor Blade

Daisaku Inoyama

Embry-Riddle Aeronautical University - Daytona Beach

Follow this and additional works at: <https://commons.erau.edu/db-theses>



Part of the [Aerospace Engineering Commons](#)

Scholarly Commons Citation

Inoyama, Daisaku, "Vibration Analysis of a Fan/Compressor Blade" (2003). *Theses - Daytona Beach*. 88.
<https://commons.erau.edu/db-theses/88>

This thesis is brought to you for free and open access by Embry-Riddle Aeronautical University – Daytona Beach at ERAU Scholarly Commons. It has been accepted for inclusion in the Theses - Daytona Beach collection by an authorized administrator of ERAU Scholarly Commons. For more information, please contact commons@erau.edu.

Vibration Analysis of a Fan/Compressor Blade

by
Daisaku Inoyama

A Thesis Submitted to the Aerospace Engineering
Department in Partial Fulfillment of the Requirements for
the Degree of Master of Science in Aerospace Engineering

Embry Riddle Aeronautical University
College of Engineering
Daytona Beach, Florida
Fall 2003

UMI Number: EP32077

INFORMATION TO USERS

The quality of this reproduction is dependent upon the quality of the copy submitted. Broken or indistinct print, colored or poor quality illustrations and photographs, print bleed-through, substandard margins, and improper alignment can adversely affect reproduction.

In the unlikely event that the author did not send a complete manuscript and there are missing pages, these will be noted. Also, if unauthorized copyright material had to be removed, a note will indicate the deletion.

UMI[®]

UMI Microform EP32077
Copyright 2011 by ProQuest LLC
All rights reserved. This microform edition is protected against
unauthorized copying under Title 17, United States Code.

ProQuest LLC
789 East Eisenhower Parkway
P.O. Box 1346
Ann Arbor, MI 48106-1346


Vibration Analysis of a Fan/Compressor Blade


By
Daisaku Inoyama

This thesis was prepared under the direction of the candidate's thesis committee chair, Dr. Habib Eslami, Department of Aerospace Engineering, and has been approved by the members of his thesis committee. It was submitted to the Department of Aerospace Engineering and was accepted in partial fulfillment of the requirements for the degree of Master of Science in Aerospace Engineering.


THESIS COMMITTEE:


Dr. Habib Eslami
Chair


Dr. Yi Zhao
Member


Dr. Siva Seenith
Member


Dr. Swami
Program Chair, MSAE Program


Department Chair, Aerospace Engineering

Copyright by Daisaku Inoyama 2003

All Rights Reserved

Acknowledgement

I would like to express sincere appreciation to my thesis advisor Dr. Habib Eslami for his guidance, knowledge, and insight. Dr. Eslami was very supportive of this thesis and has provided me with many helpful advices from his professional experience in the finite element vibration analysis. I would also appreciate Dr. James Ladesic and Dr. Frank Radosta for their assistance on MSC.PATRAN/NASTRAN operations and numerous useful advices. In addition, I would like to express special thanks to thesis committee members, Dr. Yi Zhao and Dr. Siva Seenith.

I would like to thank my parents, Masayuki Inoyama and Ayako Inoyama for their generous support. I would like to say, “thanks” to my friends, Manish Pantha, Raphaël Cioffi, Hubert Schouten, and Wasu Schouten for being there for me all the time. Most importantly, I would like to thank my wife, Kamala, for her patience and kind support throughout the writing of this thesis.

Abstract

Author: Daisaku Inoyama
Title: Vibration Analysis of a Fan/Compressor Blade
Institution: Embry Riddle Aeronautical University
Degree: Master of Science in Aerospace Engineering
Year: 2003

The vibration of blades in gas turbine engines has become an important issue during the last decade because of its significant impact on high cycle fatigue failure due to resonant vibrations. The main objective of this thesis is the vibration analysis of compressor/fan blade using three-dimensional finite element analysis together with various analytical approaches. First, the analytical solutions were established using various analytical methods, Bernoulli-Euler, Rayleigh, Rayleigh-Ritz, two-dimensional plate, and Timoshenko beam methods. Then, the vibration behaviors of the blade are analyzed in full extent using commercially available finite element solver, MSC.NASTRAN, and correlated with the analytical solutions. The finite element analysis was performed in three different models, straight plate, tapered solid, and blade models. Finally, the recommendations are made for more accurate finite element modeling and analysis procedures.

Table of Contents

Acknowledgement	iv
Abstract	v
Table of Contents	vi
List of Figures	ix
List of Tables	xi
Chapter 1: Introduction	1
1.1 Problem Statement	1
1.2 Objective of the Research	2
1.3 Blade Geometry and Material	2
Chapter 2: Background	4
2.1 Applications of Vibration Analysis	4
2.2 Natural Frequencies of Rotating Blades	4
2.3 Current Research Efforts	5
Chapter 3: Theory	7
3.1 Analytical Approach	7
3.1.1 Approximation of Blade Geometry as a Uniform Cantilever Beam	7
3.1.2 Bernoulli-Euler Beam Method	9
3.1.3 Timoshenko Beam Theory	15
3.1.4 Approximation of Blade: Tapered Beam with a Concentrated Mass	19
3.1.5 Approximate Method	21
3.1.6 Rayleigh's Method	22
3.1.7 Rayleigh-Ritz Method	27

3.1.8 Two Dimensional Plate Method	33
3.2 Finite Element Approach	36
3.2.1 Equation of Motion	37
3.2.2 Normal Modes Analysis	38
Chapter 4: Finite Element Analysis Procedures	40
4.1 Finite Element Modeling Procedures.....	40
4.1.1 Importing Geometric Model into Finite Element Modeler.....	40
4.1.2 Geometric Modification.....	42
4.1.3 Meshing of the Blade	44
4.1.4 Blade Material Property, Element Property, and Constraint Definition.....	45
4.1.5 Mesh Examination and Remeshing	46
4.2 Finite Element Analysis.....	47
4.2.1 Creating Analysis File.....	47
4.2.2 Running Analysis.....	48
4.2.3 Importing and Obtaining Results	48
Chapter 5: Results	49
5.1 Analytical Solution	49
5.1.1 Bernoulli-Euler Beam Method.....	50
5.1.2 Solution of the Timoshenko Beam Theory	52
5.1.3 Solution of the Rayleigh's Method	52
5.1.4 Rayleigh-Ritz Method.....	54
5.1.5 Two-Dimensional Plate Method.....	57
5.2 Finite Element Solution	59

5.2.1: Plate Finite Element Solution	60
5.2.2 Finite Element Solution of Tapered Solid Model	61
5.2.3 Finite Element Solution of the Blade Model	62
5.2.4 Close Examination of the Plate Finite Element Solution.....	65
5.2.5 Close Examination of the Tapered Solid Finite Element Solution.....	75
5.2.6 Close Examination of the Blade Finite Element Solution	85
Chapter 6: Conclusion.....	96
Chapter 7: Recommendation.....	98
7.1 Effect of Blade and Rotor Joints.....	98
7.2 Gap Contacts between Blade Attachments	99
7.3 Forced Vibration Analysis and Computational Fluid Dynamics (CFD)	99
7.4 Aerodynamic and Structural Damping	100
References.....	102
Appendix: Eigenvalue Extraction Methods	103
A1 Lanczos Method.....	104
A2 Givens and Householder Method.....	104
A3 Modified Givens and Modified Householder Methods	105
A4 Inverse Power Method	105
A5 Sturm Modified Inverse Power Method.....	106

List of Figures

Figure 1.1: Geometry of an actual blade.....	3
Figure 3.1: Uniform cantilever beam model.....	4
Figure 3.2: Transverse vibration considering rotary inertia and shear deformation....	16
Figure 3.3: Influence of rotary inertia and shear deformation.....	19
Figure 3.4: Tapered beam with a concentrated mass model.....	20
Figure 3.5: Two-dimensional flat plate model.....	33
Figure 3.6: Single degree-of-freedom model.....	38
Figure 4.1: Imported blade model.....	42
Figure 4.2: Modified blade model.....	45
Figure 4.3: Meshed blade model.....	46
Figure 5.1: Mode 1 of plate model.....	65
Figure 5.2: Mode 2 of plate model.....	66
Figure 5.3: Mode 3 of plate model.....	67
Figure 5.4: Mode 4 of plate model.....	68
Figure 5.5: Mode 5 of plate model.....	69
Figure 5.6: Mode 6 of plate model.....	70
Figure 5.7: Mode 7 of plate model.....	71
Figure 5.8: Mode 8 of plate model.....	72
Figure 5.9: Mode 1 of tapered solid model.....	75
Figure 5.10: Mode 2 of tapered solid model.....	76
Figure 5.11: Mode 3 of tapered solid model.....	77
Figure 5.12: Mode 4 of tapered solid model.....	78

Figure 5.13: Mode 5 of tapered solid model.....	79
Figure 5.14: Mode 6 of tapered solid model.....	80
Figure 5.15: Mode 7 of tapered solid model.....	81
Figure 5.16: Mode 8 of tapered solid model.....	82
Figure 5.17: Mode 1 of blade model.....	85
Figure 5.18: Mode 2 of blade model.....	86
Figure 5.19: Mode 3 of blade model.....	87
Figure 5.20: Mode 4 of blade model.....	88
Figure 5.21: Mode 5 of blade model.....	89
Figure 5.22: Mode 6 of blade model.....	90
Figure 5.23: Mode 7 of blade model.....	91
Figure 5.24: Mode 8 of blade model.....	92

List of Tables

Table 3.1: First eight eigenvalues (λ^2 's) of the cantilever plate equation.....	35
Table 5.1: Summary of the Bernoulli-Euler solution.....	51
Table 5.2: Summary of the Rayleigh's method solution.....	53
Table 5.3: Summary of the Rayleigh-Ritz solution.....	56
Table 5.4: Summary of the analytical two-dimensional plate solution	59
Table 5.5: Comparison: the analytical plate solution and the plate FEA solution.....	60
Table 5.6: Comparison: the Rayleigh's method and the tapered solid FEA solutions..	62
Table 5.7: Comparison: the plate FEA and the blade FEA solutions.....	63
Table 5.8: Comparison: the tapered solid FEA and the blade FEA solutions.....	64

Chapter 1

Introduction

1.1 Problem Statement

Since the first modern gas turbine engine was invented in the early last century, the technology involving a “jet” engine has evolved dramatically. One of the major problems that the engineers encountered in the early development stage was the blade vibration. Although the theory of structural dynamics was well understood at the time, an effective method of determining natural frequencies of the blade and the associated mode shapes was not available until the finite element analysis was developed in the mid 1970’s. Dramatic increase in the development of high power computers and rapidly increasing capacity for more precise computation of engineering problems during past few decades contributed to the capability of utilizing three-dimensional (3-D) finite element analysis that could not have been easily implemented before. Using the modern computers, the finite element analysis can be performed efficiently to solve for natural frequencies and vibration mode shapes of structures with complex geometry, such as a rotating fan/compressor blade. In recent years, the vibration of blades has become an increasingly important design factor due to its significant impact on high cycle fatigue failure, especially for the jet engine installed in the aircraft, where the safety is a major concern. It is necessary, therefore, to determine the natural frequencies of blades in gas turbine engine and fully understand their vibration behavior to avoid a devastating resonant vibration.

1.2 Objective of the Research

The main focus of this thesis is to perform a three-dimensional (3-D) finite element analysis on a real fan/compressor blade in order to determine its natural frequencies. Consequently, the effectiveness of the finite element analysis for the vibration problem can be reinforced by various analytical methods. In addition to the determination of natural frequencies, mode shapes and location of nodes can be visually examined by computer simulations.

To accomplish these objectives, the professionally available finite element codes, MSC.NASTRAN, and the finite element modeler, MSC.PATRAN are utilized. The major advantage of the finite element method is that the natural frequencies of blades can be determined exclusively without having to conduct a mechanical vibration testing.

In order to understand the behavior of the blade under free vibration, the blade is modeled as a simple cantilever beam and as a thin flat plate at the beginning. Natural frequencies of those simple models are determined using various analytical methods, the exact and the approximate methods. The analytical reference that can be compared with the finite element solution to verify the reliability of finite element analysis on such a vibration problem is established using solutions from those analytical methods.

1.3 Blade Geometry and Material

The fan/compressor blade analyzed for this research project has a very complex geometry with irregular surfaces. The overall length of the blade is approximately 0.411 m and the width at the mid-length is approximately 0.1385 m. The blade is comprised of irregular surfaces with numerous curves and twisted from bottom to the top. Maximum

thickness at the bottom is approximately 0.0155 m and at the top is approximately 0.0032 meter. The blade is made of the titanium alloy with elastic modulus of 118.3 GPa, shear modulus of 42.1 GPa, Poisson's ratio of 0.342, and mass density of 4430 kg/m³. The actual blade is shown below.

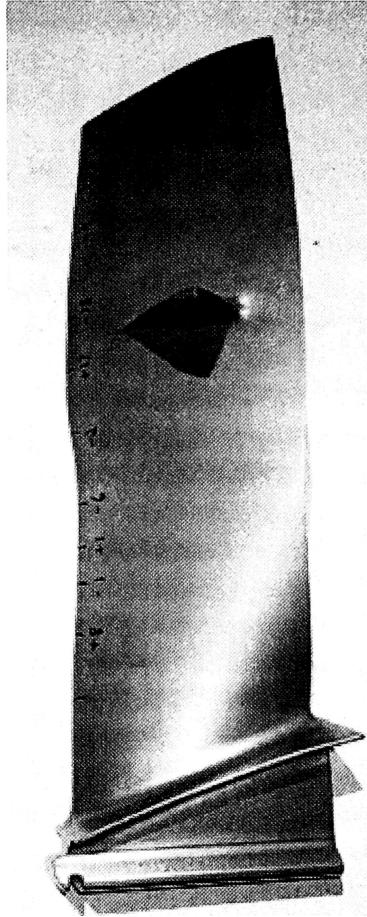


Figure 2.1: Geometry of an actual blade

Chapter 2

Background

2.1 Applications of Vibration Analysis

Vibration analysis is extremely important for many reasons. The vibration of structures is among the key research areas in aerospace engineering, mechanical engineering, civil engineering and other related disciplines. Vibration analysis that includes determination of natural frequencies (normal mode analysis) and behaviors of structures under forced vibration (forced vibration analysis) is vital to many industrial applications. In addition, one of the major elements of structural designs is to overcome the structural resonance and meet the requirements of the design objectives that include low-noise, durability, and reliability

2.2 Natural Frequencies of Rotating Blades

The blade vibration has been recognized as one of the major causes of high cycle fatigue failure in gas turbine engine. Since compressor/fan blades are continuously excited by rotational and aerodynamic forces throughout the engine operation, it is imperative to study the response of blades to such excitation forces. If the frequency of the excitation force coincides with the natural frequency of blade during the normal engine operation range, high amplitude vibration may occur and the resulting stress on the blade may cause a catastrophic failure. Therefore, all of the rotating blades shall be verified and investigated for natural frequencies to avoid harmful resonant vibration.

2.3 Current Research Efforts

Over the past few decades, numerous researches were conducted over the subject of blade vibration. In 1996, Kruse and Pierre of University of Michigan at Ann Arbor studied the dynamic response of an industrial turbomachinery rotor and blades [6]. They utilized three-dimensional finite element models to investigate the free and forced vibration of a rotor and blades of gas turbine engine. The researchers have successfully utilized MSC.NASTRAN to study the free vibration natural frequencies of complex structures, such as a combined model of a rotor disk and blades.

Furthermore, Jian Hou from Aeronautical and Maritime Research Laboratory in Australia conducted a vibration analysis on the bladed rotor of gas turbine engine [7]. Hou utilized the three-dimensional finite element methods to determine the natural frequencies of rotating blades with various types of geometric constraints. The three-dimensional finite element analysis effectively revealed the variations in the natural frequencies as the constraint conditions are changed. Hou has examined the natural frequencies of several blade-rotor models with different boundary conditions, such as free-free, fixed-free, and flexibly fixed-free constraints.

Recently, several researchers (Fleeter, Zhou, Houstis, and Rice) from Purdue University conducted a research on high cycle fatigue (HCF) of a turbomachinery blade due to the resonant vibratory stresses [16]. Their approach involved the use of three-dimensional finite element analysis to determine the natural frequencies and vibration modes of the blade. In addition, forcing functions as a result of the rotor movement was applied to the model in order to predict the vibratory stresses for various rotor speeds. In addition, researchers utilized a computational fluid dynamics (CFD) to determine the

aerodynamic damping and the aerodynamic forcing functions acting on the finite element model to accurately predict the total resonant vibratory stresses.

Chapter 3

Theory

3.1 Analytical Approach

The analytical approach can only be used to solve natural frequencies of a geometrically simple structure. Thus, it is not possible to determine the natural frequencies of the actual blade model by using the analytical methods unless an equivalent approximated model with a simple geometry is obtained. Various theoretical techniques can be applied to this simple model in order to calculate its natural frequencies and mode shapes. In this thesis, the model is first assumed to be a simple cantilever beam and its natural frequencies are computed using Bernoulli-Euler method. Then, the Timoshenko beam theory is presented to correct the error in the Bernoulli-Euler solution. Approximate methods, such as Raleigh method and Rayleigh-Ritz method, are utilized to solve for natural frequencies of more complex analytical model, such as the one with concentrated mass placed at the intermediate location. Finally, the model is approximated as a two-dimensional plate clamped at one side and free at the other sides (cantilever plate). The two-dimensional plate vibration theory is presented to gain more accuracy in the analytical solution.

3.1.1 Approximation of Blade Geometry as a Uniform Cantilever Beam

An accurate approximation of the blade geometry is one of the most important processes to obtain accurate analytical solution. For Bernoulli-Euler method, the analytical model must have a constant thickness and width as it is considered as a uniform beam. Therefore, the thickness of the beam model is set to be the average

thickness of the actual blade. This average thickness of the blade is determined by taking an average across the width of the blade and, then, taking an average of this value across the length of the blade. The calculation process is shown as follows.

Using the measurement taken from the actual blade, the average thickness at the fixed bottom of the actual blade (blade root) is determined,

$$T_{ave-b} = \frac{T_{Max-b} + T_{Min-b}}{2} \quad (3.1)$$

Similarly, at the mid-length of the blade

$$T_{ave-m} = \frac{T_{Max-m} + T_{Min-m}}{2} \quad (3.2)$$

At the top (blade tip) of the blade, the average thickness is,

$$T_{ave-t} = \frac{T_{Max-t} + T_{Min-t}}{2} \quad (3.3)$$

Then, the average blade thickness is determined as,

$$T_{ave} = \frac{T_{ave-b} + T_{ave-m} + T_{ave-t}}{3} \quad (3.4)$$

This average thickness of the blade serves as the uniform thickness of the cantilever beam model. It is not necessary to determine the average width of the blade, since it is nearly constant along entire blade length. Therefore, the width of a beam (W) is considered the same as the middle section width of the blade. With those dimensions available, cross sectional area of the beam can be determined by $A = T_{ave} W$ and the moment inertia of the beam is $I = \frac{1}{12} W T_{ave}^3$ for the rectangular cross section. This method to represent an actual blade as a uniform beam model may sound somewhat unreliable, but it will be proven later that the method is actually valid and fairly accurate.

3.1.2 Bernoulli-Euler Beam Method

The transverse vibration of the beam can be analyzed by using the Bernoulli-Euler beam method, where the deflection $y(x,t)$ of the beam is due to the bending moment only and no considerations are made for rotary inertia and shear deformation. It is known that this theory is especially effective when the length-to-width ratio is greater than or equal to 10 [1]. Bernoulli-Euler method can still provide an acceptable result down to about length-to-width ratio of 3. Since the blade being analyzed in this thesis has the length-width ratio of about 3, it can be considered as a slender beam and, therefore, the beam theory is applicable.

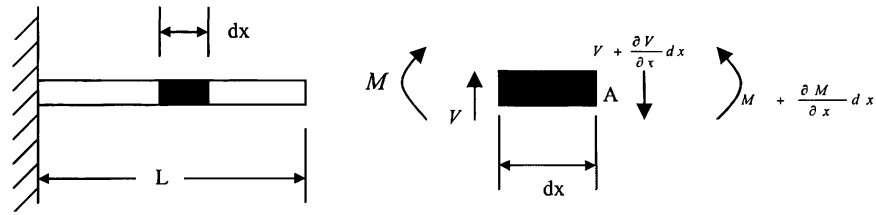


Figure 3.1: Uniform cantilever model

A differential element dx of the beam is shown above in Figure 3.1. This figure illustrates the bending moments M and shear forces V acting upon it. As the beam vibrates, the differential element dx moves vertically up and down in the y direction and also rotates slightly. By summing the forces in the y -direction yields the formulation below.

$$+\uparrow \sum F = (\Delta m)a_y \quad (3.5)$$

where, $\Delta m = \rho A dx$ and $a_y = \frac{\partial^2 y}{\partial t^2}$

$$+\uparrow \sum F = \rho A dx \frac{\partial^2 y}{\partial t^2} \quad (3.6)$$

$$V - V - \frac{\partial V}{\partial x} dx = \rho A dx \frac{\partial^2 y}{\partial t^2} \quad (3.7)$$

Simplification of Eq.(3.3) allows,

$$-\frac{\partial V}{\partial x} = \rho A \frac{\partial^2 y}{\partial t^2} \quad (3.8)$$

Now, ignoring the rotary inertia and summing the moments about points A yields,

$$\sum M_A = 0 \quad (3.9)$$

$$-M - Vdx + M + \frac{\partial M}{\partial x} dx = 0 \quad (3.10)$$

$$Vdx = \frac{\partial M}{\partial x} dx \quad (3.11)$$

$$V = \frac{\partial M}{\partial x} \quad (3.12)$$

For a linearly elastic beam,

$$M = \frac{EI}{\mu} \quad (3.13)$$

where, μ is the curvature of elastic curve.

From solid mechanics, bending moment is a function of the change in slope of the beam's elastic curve. For small slope,

$$M = EI \left(\frac{\partial^2 y}{\partial x^2} \right) \quad (3.14)$$

Substitution of Eq.(3.14) into Eq.(3.12) allows,

$$V = \frac{\partial}{\partial x} \left(EI \frac{\partial^2 y}{\partial x^2} \right) \quad (3.15)$$

Then, substituting Eq.(3.15) into Eq.(3.8) results in,

$$-\frac{\partial^2}{\partial x^2} \left(EI \frac{\partial^2 y}{\partial x^2} \right) = \rho A \frac{\partial^2 y}{\partial t^2} \quad (3.16)$$

Considering EI to be constant, Eq.(3.16) becomes,

$$EI \frac{\partial^4 y}{\partial x^4} + \rho A \frac{\partial^2 y}{\partial t^2} = 0 \quad (3.17)$$

Rearranging this equation to obtain,

$$\frac{\partial^4 y}{\partial x^4} + \left(\frac{\rho A}{EI} \right) \frac{\partial^2 y}{\partial t^2} = 0 \quad (3.18)$$

$$\frac{\partial^4 y}{\partial x^4} + \frac{1}{C^2} \frac{\partial^2 y}{\partial t^2} = 0 \quad (3.19)$$

where, $C = \sqrt{\frac{EI}{\rho A}}$. Rearrange the above equation to obtain,

$$-\frac{\partial^4 y}{\partial x^4} = \frac{1}{C^2} \frac{\partial^2 y}{\partial t^2} \quad (3.20)$$

Equation (3.20) is the one-dimensional wave equation. This partial differential equation can be solved by the technique known as the separation of variables. Assume the displacement $y(x,t)$ to be the product of two single-variable functions:

$$y(x,t) = X(x)T(t) \quad (3.21)$$

Differentiating Eq.(3.21) four times with respect to x ,

$$\frac{\partial^4 y}{\partial x^4} = \frac{d^4 X(x)}{dx^4} T(t) \quad (3.22)$$

Also, differentiating Eq.(3.21) twice with respect to t ,

$$\frac{\partial^2 y}{\partial t^2} = \frac{d^2 T(t)}{dt^2} X(x) \quad (3.23)$$

Substitute Eq.(3.22) and Eq.(3.23) into Eq.(3.20),

$$-\frac{d^4 X(x)}{dx^4} T(t) = \frac{1}{C^2} X(x) \frac{d^2 T(t)}{dt^2} \quad (3.24)$$

Rearrange Eq.(3.24) and form two ordinary differential equations,

$$-\frac{d^4 X(x)}{dx^4} \frac{C^2}{X(x)} = K \quad (3.25)$$

and,

$$\frac{d^2 T(t)}{dt^2} \frac{1}{T(t)} = K \quad (3.26)$$

where, K is an arbitrary constant. For convenience and to avoid a trivial solution,

$$K = -\omega_n^2 \quad (3.27)$$

Then, the two ordinary differential equations become,

$$\frac{d^4 X(x)}{dx^4} - \frac{\omega_n^2}{C^2} X(x) = 0 \quad (3.28)$$

and,

$$\frac{d^2 T(t)}{dt^2} + \omega_n^2 T(t) = 0 \quad (3.29)$$

Assume two solutions of Eq.(3.21) to be,

$$T(t) = B_1 \sin(\omega t) + B_2 \cos(\omega t) \quad (3.30)$$

$$X(x) = D e^{\lambda x} \quad (3.31)$$

Differentiate Eq.(3.31) four times with respect to x to obtain,

$$\frac{d^4 X(x)}{dx^4} = D \lambda^4 e^{\lambda x} \quad (3.32)$$

Substitute Eq.(3.31) and Eq.(3.32) to Eq.(3.28) to obtain,

$$D \lambda^4 e^{\lambda x} - \frac{\omega_n^2}{C^2} D e^{\lambda x} = 0 \quad (3.33)$$

Simplify above equation to obtain auxiliary equation,

$$\lambda^4 - \frac{\omega_n^2}{C^2} = 0 \quad (3.34)$$

Let $N^4 = \frac{\omega_n^2}{C^2}$,

$$\lambda^4 - N^4 = 0 \quad (3.35)$$

There are four roots for the above equation,

$$\lambda_1 = N \quad (3.36a)$$

$$\lambda_2 = -N \quad (3.36b)$$

$$\lambda_3 = iN \quad (3.36c)$$

$$\lambda_4 = -iN \quad (3.36d)$$

Then, the Eq.(3.31) becomes,

$$X(x) = D_1 e^{Nx} + D_2 e^{-Nx} + D_3 e^{iNx} + D_4 e^{-iNx} \quad (3.37)$$

Apply trigonometric relationships to transform above equation,

$$X(x) = D_1 \sinh(Nx) + D_2 \cosh(Nx) + D_3 \sin(Nx) + D_4 \cos(Nx) \quad (3.38)$$

Although constants of the Eq.(3.37) and Eq.(3.38) are actually different, they are identified using the same characters for simplicity. Now, combine Eq.(3.30) and Eq.(3.38) to obtain a general solution,

$$y(x, t) = (B_1 \sin(\omega t) + B_2 \cos(\omega t))(D_1 \sinh(Nx) + D_2 \cosh(Nx) + D_3 \sin(Nx) + D_4 \cos(Nx)) \quad (3.39)$$

To determine natural frequencies, consider Eq.(3.38) and apply boundary conditions for cantilever beam,

$$X(0) = 0 \quad (3.40)$$

$$\frac{dX(0)}{dx} = 0 \quad (3.41)$$

$$\frac{d^2 X(L)}{dx^2} = 0 \quad (3.42)$$

$$\frac{d^3 X(L)}{dx^3} = 0 \quad (3.43)$$

It is obvious that four boundary conditions that represent the fixed end and the stress-free end are required, since there are four unknown constants. After application of those boundary conditions, Eq.(3.38) can be expressed in the matrix form,

$$\begin{bmatrix} 0 & 1 & 0 & 1 \\ N & 0 & N & 0 \\ N^2 \sinh(NL) & N^2 \cosh(NL) & -N^2 \sin(NL) & -N^2 \cos(NL) \\ N^3 \cosh(NL) & N^3 \sinh(NL) & -N^3 \cos(NL) & -N^3 \sin(NL) \end{bmatrix} \begin{Bmatrix} D_1 \\ D_2 \\ D_3 \\ D_4 \end{Bmatrix} = \{0\} \quad (3.44)$$

For the above matrix equation to be non-trivial, the determinant of the coefficients must vanish. Then,

$$\det \begin{bmatrix} 0 & 1 & 0 & 1 \\ N & 0 & N & 0 \\ N^2 \sinh(NL) & N^2 \cosh(NL) & -N^2 \sin(NL) & -N^2 \cos(NL) \\ N^3 \cosh(NL) & N^3 \sinh(NL) & -N^3 \cos(NL) & -N^3 \sin(NL) \end{bmatrix} = \{0\} \quad (3.45)$$

This will lead to the characteristic equation:

$$\cos(NL) \cosh(NL) + 1 = 0 \quad (3.46)$$

To solve this equation for (NL) which is the eigenvalue times the length, numerical computation must be performed using a computer,

$$(NL)_1 = 1.8751 \quad (3.47a)$$

$$(NL)_2 = 4.6941 \quad (3.47b)$$

$$(NL)_3 = 7.8548 \quad (3.47c)$$

Using $N^4 = \frac{\omega_n^2}{C^2}$ and $C = \sqrt{\frac{EI}{\rho A}}$,

$$N^4 = \frac{\omega_n^2}{C^2} = \frac{\rho A \omega_n^2}{EI} \quad (3.48)$$

Rearrange above equation and multiply by $\frac{L^2}{L^2}$ to obtain,

$$\omega_n = \frac{(NL)_n^2}{L^2} \sqrt{\frac{EI}{\rho A}} \quad (3.49)$$

This is the equation for natural frequencies derived using Bernoulli-Euler beam method. This equation always results in the positive definite solution and can be easily used to compute natural frequencies.

3.1.3 Timoshenko Beam Theory

Timoshenko beam theory accounts for both the effect of rotary inertial and shear deformation that are neglected in case of Bernoulli-Euler beam method [1]. With these considerations, Timoshenko beam theory is applicable to the determination of natural frequencies of a thick beam with small length-width ratio. In addition, Timoshenko beam theory is useful for the analysis of high frequency vibration where the effect of rotary inertia and shear deformation may be significant. Since the uniform beam model analyzed using Bernoulli-Euler method has a fairly small length-width ratio, it is beneficial to utilize the Timoshenko beam theory to correct the error that may be present

in the solution. A differential element dx is shown in Figure 3.2 to illustrate the rotation and deformation of the beam in addition to the transverse motion.

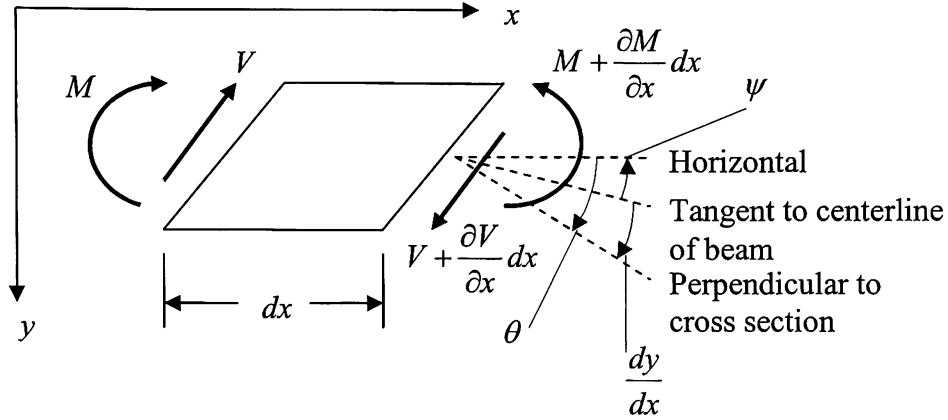


Figure 3.2: Transverse vibration considering rotary inertia and shear deformation

As shown in Figure 3.2, as a beam undergoes transverse vibration, a differential element will rotate in addition to its translational motion. The angle of rotation is equal to the slope of the elastic curve, $\frac{\partial y}{\partial x}$. Then, the corresponding angular acceleration is given as,

$$\frac{\partial^3 y}{\partial x \partial t^2} \quad (3.50)$$

Thus, the inertial moment of the differential element about an axis passing through its mass center and perpendicular to the x-y plane is,

$$-\rho I \frac{\partial^3 y}{\partial x \partial t^2} dx \quad (3.51)$$

where, I is the moment of inertia of the cross section. The governing differential equation of the beam, Eq.(3.17), can, therefore, be modified to account for rotary inertial by including Eq.(3.51). The governing differential equation of the beam becomes,

$$EI \frac{\partial^4 y}{\partial x^4} + \rho A \frac{\partial^2 y}{\partial t^2} - \rho I \frac{\partial^3 y}{\partial x \partial t^2} dx = 0 \quad (3.52)$$

The slope of the deflection curve will depend upon shearing deformations as well as on rotation of the cross section. In Figure 3.2, θ represents the slope of the deflection curve without the consideration of shear deformation and ψ is the angle of shear at the neutral axis. Then, the slope of the deflection curve due to both shear force and bending moment can be written as,

$$\frac{dy}{dx} = \theta + \psi \quad (3.53)$$

Where,

$$\psi = \frac{V}{kAG} \quad (3.54)$$

A = cross-sectional area of the beam

G = modulus of rigidity

k = Timoshenko's shear coefficient, dependent on the shape of the cross-section

Timoshenko's shear coefficient is the given constant. For the rectangular cross section, the coefficient, k , is given as $\frac{5}{6}$. Summing the moment at the right edge of the

differential element in Figure 3.2 with consideration of rotary inertia,

$$Vdx - \frac{\partial M}{\partial x} dx - \rho I \frac{\partial^2 \theta}{\partial t^2} dx = 0 \quad (3.55)$$

where, by definition,

$$M = -EI \frac{d\theta}{dx} \quad (3.56)$$

and,

$$V = k\psi AG = kAG \left(\frac{dy}{dx} - \theta \right) \quad (3.57)$$

Substituting Eq.(3.56) and Eq.(3.57) into Eq.(3.55) allows the differential equation for rotation,

$$EI \frac{\partial^2 \theta}{\partial x^2} + kAG \left(\frac{\partial y}{\partial x} - \theta \right) - \rho I \frac{\partial^2 \theta}{\partial t^2} = 0 \quad (3.58)$$

Summing the force in the vertical direction allows,

$$\frac{\partial V}{\partial x} - \rho A \frac{\partial^2 \theta}{\partial t^2} = 0 \quad (3.59)$$

Applying Eq.(3.57) to the above equation allows the differential equation for the transverse motion.

$$kG \left(\frac{\partial^2 y}{\partial x^2} - \frac{\partial \theta}{\partial x} \right) - \rho \frac{\partial^2 y}{\partial t^2} = 0 \quad (3.60)$$

By solving Eq.(3.60) for $\frac{\partial \theta}{\partial x}$ and substituting the result in Eq.(3.58), the equation of

motion for the beam can be formed as,

$$EI \frac{\partial^4 y}{\partial x^4} + \rho A \frac{\partial^2 y}{\partial t^2} - \rho I \left(1 + \frac{E}{kG} \right) \frac{\partial^4 y}{\partial x^2 \partial t^2} + \frac{\rho^2 I}{kG} \frac{\partial^4 y}{\partial t^4} = 0 \quad (3.61)$$

For cantilever beam, boundary conditions are given as follows.

Fixed end:

$$\theta = y = 0 \quad (3.62a)$$

Free end:

$$kAG \left(\frac{\partial y}{\partial x} - \theta \right) = EI \frac{\partial \theta}{\partial x} = 0 \quad (3.62b)$$

Since the solution of Eq.(3.61) with boundary conditions, Eq.(3.62a) and Eq.(3.62b), cannot be obtained easily and the resulting frequency equation is rather complex, a graph showing the influence of shear deformation and rotary inertia is presented below [].

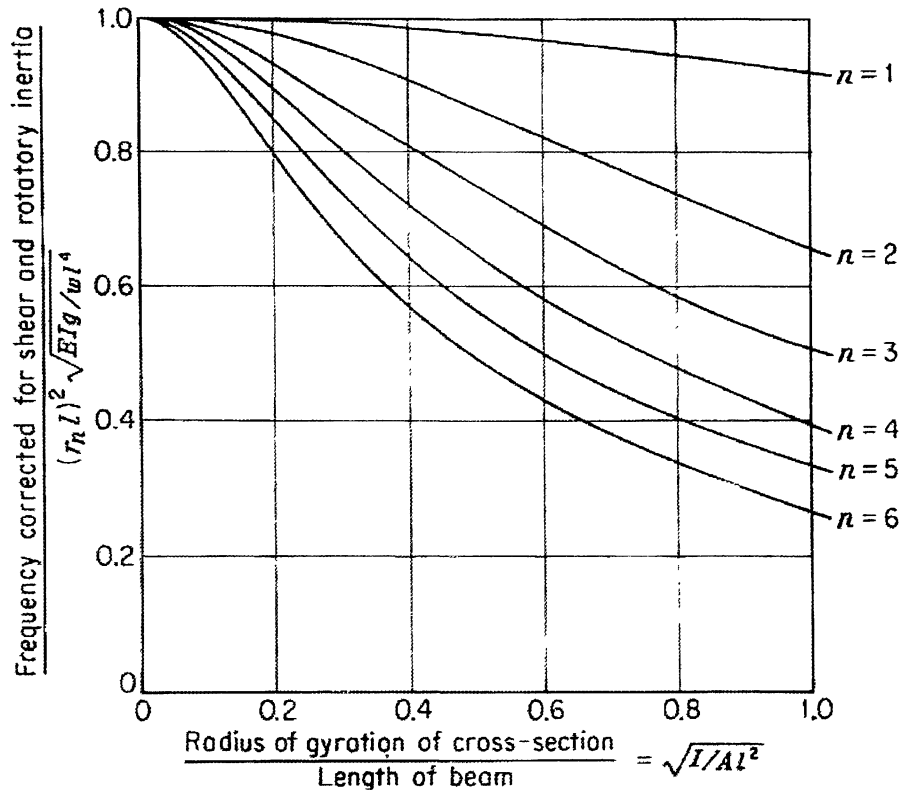


Figure 3.3: Influence of rotary inertia and shear deformation on natural frequencies of a cantilever beam (From J.G. Sutherland and L.E. Goodman Technical Report)

3.1.4 Approximation of Blade: Tapered Beam with a Concentrated Mass

The continuous systems discussed thus far have simple geometry with a simple governing equation. This simple system could be solved by an exact analytical method, using Bernoulli-Euler beam theory. It is obvious that this simple uniform beam may not show the clear picture of the actual behavior of the blade. Therefore, more desirable results may be obtainable by assuming the blade to be a mildly tapered beam with a

concentrated mass. The concentrated mass represents two protruding figures at the middle of the blade.

The averaging procedure of blade thickness is similar to the one of uniform beam. The average thickness across the width is taken at the bottom and the top of the blade. These average thicknesses of blade are considered as the thickness of beam at the top and bottom. Beam thickness at the bottom linearly tapers down to the one at the top. As mentioned previously, width of the beam is considered constant, since it does not differ significantly throughout the entire length of the actual blade. The tapered beam model is shown below.

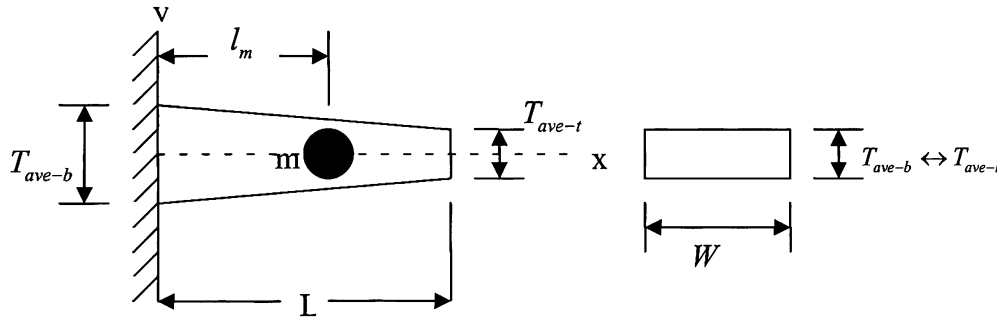


Figure 3.4: Tapered beam with a concentrated mass model

Average thickness at the bottom is determined by,

$$T_{ave-b} = \frac{T_{Max-b} + T_{Min-b}}{2} \quad (3.63)$$

Similarly for the top,

$$T_{ave-t} = \frac{T_{Max-t} + T_{Min-t}}{2} \quad (3.64)$$

Then, the variation of the thickness along beam length can be expressed as,

$$T(x) = \left(T_{ave-b} - \frac{T_{ave-b} - T_{ave-t}}{L} x \right) \quad (3.65)$$

Also, the cross sectional area of the beam can be expressed as,

$$A(x) = T(x)W = \left(T_{ave-b} - \frac{T_{ave-b} - T_{ave-t}}{L} x \right) W \quad (3.66)$$

Since the cross sectional shape of the beam is rectangle, the moment of inertia can be obtained using,

$$I(x) = \frac{1}{12} W [T(x)]^3 \quad (3.67)$$

substituting Eq.(3.65) into the above equation,

$$I(x) = \frac{1}{12} W \left(T_{ave-b} - \frac{T_{ave-b} - T_{ave-t}}{L} x \right)^3 \quad (3.68)$$

Expand above equation and simplify to obtain,

$$I(x) = \frac{1}{12} W \left(T_{ave-b}^3 - 3T_{ave-b}^2 \left(\frac{T_{ave-b} - T_{ave-t}}{L} \right) x + T_{ave-b} \left(\frac{T_{ave-b} - T_{ave-t}}{L} \right)^2 x^2 + \left(\frac{T_{ave-b} - T_{ave-t}}{L} \right)^3 x^3 \right) \quad (3.69)$$

This is the equation for moment of inertia for the tapered beam. Next, the Rayleigh and Rayleigh-Ritz methods are employed to estimate natural frequencies of the beam.

3.1.5 Approximate Method

Exact solutions can only be obtained for beams with simple geometry. Unfortunately, exact solutions for the vibration of continuous systems with complex geometry may not be available for most practical purposes [10]. Therefore, an approximate method must be utilized for a continuous system that carries a concentrated mass and has a non-uniform geometry.

In case of the blade geometry in this thesis, it is obvious that the best analytical solution can be obtained by assuming the concentrated mass at the middle section of the blade where two protruding geometries are present. In addition, the actual blade does not have a constant thickness along its length and should be modeled as a tapered beam instead of a uniform beam. Finally, as mentioned previously, Bernoulli-Euler theory is known to provide a good solution only in case of slender beam and should not be applied when the length-width ratio requirement is not met. Although the blade is considered ‘fairly’ slender (L/W between 3 and 10), the exact solution obtained by Bernoulli-Euler theory should, at least, be verified by an approximate method.

3.1.6 Rayleigh’s Method

The Rayleigh’s method is an approximate method useful in estimating the first natural frequency of an undamped continuous system [10]. The disadvantage of this method is its incapability in determining the higher natural frequencies and mode shapes of vibration. Although Rayleigh’s method may not be the best choice of approximate method due to those drawbacks, it is considered as the basis for the majority of approximate techniques used in vibration analysis and, therefore, worth mentioning here. Consider the beam in Figure 3.4 and assume a general solution of transverse deflection,

$$y(x,t) = X(x)Z(t) \quad (3.70)$$

where,

$X(x)$ is the assumed deflected shape

$Z(t)$ is the time variable function

Strain energy due to transverse deformation is defined as,

$$U = \frac{1}{2} \int_0^L EI(x) \left[\frac{\partial^2 y(x,t)}{\partial x^2} \right]^2 dx \quad (3.71)$$

Substituting Eq.(3.70) to the above equation,

$$U = \frac{1}{2} [Z(t)]^2 \int_0^L EI(x) \left[\frac{\partial^2 X(x)}{\partial x^2} \right]^2 dx \quad (3.72)$$

where,

E = Modulus of elasticity

$I(x)$ = Moment of inertia

Kinetic energy of vibration is defined as,

$$V = \frac{1}{2} \int_0^L \rho A(x) \left[\frac{\partial y(x,t)}{\partial t} \right]^2 dx + \frac{1}{2} m \left[\frac{\partial y(l_m,t)}{\partial t} \right]^2 \quad (3.73)$$

Substituting Eq.(3.70) to above equation,

$$V = \frac{1}{2} \left[\frac{\partial Z(t)}{\partial t} \right]^2 \int_0^L \rho A(x) [X(x)]^2 dx + \frac{1}{2} m [X(l_m)]^2 \left[\frac{\partial Z(t)}{\partial t} \right]^2 \quad (3.74)$$

where,

ρ = Mass density

$A(x)$ = Cross sectional area of the beam

m = Concentrated mass

l_m = Distance to concentrated mass from the wall

If the free vibration is assumed to be harmonic in nature or $y = f(\sin \omega t)$, then the time

function can be expressed as,

$$Z(t) = C \sin \omega t \quad (3.75)$$

$$\frac{\partial Z(t)}{\partial t} = C \omega \cos \omega t \quad (3.76)$$

where, $Z(t) = C$

C = the amplitude at any given time

ω = circular natural frequency

For maximum $Z(t)$, $\sin \omega t$ becomes unity, then,

$$Z_{\max} = C \quad (3.77)$$

For maximum $\frac{\partial Z(t)}{\partial t}$, $\cos \omega t$ becomes unity, then,

$$\left[\frac{\partial Z(t)}{\partial t} \right]_{\max} = C\omega \quad (3.78)$$

By substituting Eq.(3.77) into Eq.(3.72), maximum strain energy can be expressed as,

$$U_{\max} = \frac{1}{2} C^2 \int_0^L EI(x) \left[\frac{\partial^2 X(x)}{\partial x^2} \right]^2 dx \quad (3.79)$$

By substituting Eq.(3.78) into Eq.(3.74), maximum kinetic energy can be expressed as,

$$V_{\max} = \frac{1}{2} C^2 \omega^2 \int_0^L \rho A(x) [X(x)]^2 dx + \frac{1}{2} m C^2 \omega^2 [X(l_m)]^2 \quad (3.80)$$

From the conservation of energy, maximum strain energy and kinetic energy must be equal,

$$V_{\max} = U_{\max} \quad (3.81)$$

Substituting Eq.(3.79) and Eq.(3.80) into the above equation allows,

$$\frac{1}{2} C^2 \omega^2 \int_0^L \rho A(x) [X(x)]^2 dx + \frac{1}{2} m C^2 \omega^2 [X(l_m)]^2 = \frac{1}{2} C^2 \int_0^L EI(x) \left[\frac{\partial^2 X(x)}{\partial x^2} \right]^2 dx \quad (3.82)$$

Simplify and above equation to obtain,

$$\omega^2 \left[\int_0^L \rho A(x) [X(x)]^2 dx + m [X(l_m)]^2 \right] = \int_0^L EI(x) \left[\frac{\partial^2 X(x)}{\partial x^2} \right]^2 dx \quad (3.83)$$

Rearrange above equation to obtain,

$$\omega^2 = \lambda_R = \frac{\int_0^L EI(x) \left[\frac{\partial^2 X(x)}{\partial x^2} \right]^2 dx}{\int_0^L \rho A(x) [X(x)]^2 dx + m [X(l_m)]^2} \quad (3.84)$$

This is the equation for the fundamental natural frequency and known as Rayleigh quotient. Assuming that deflected shape of the beam is,

$$X(x) = \left(\frac{x}{L} \right)^2 \quad (3.85)$$

$$\frac{\partial^2 X(x)}{\partial x^2} = \frac{2}{L^2} \quad (3.86)$$

Also,

$$X(l_m) = \left(\frac{l_m}{L} \right)^2 \quad (3.87)$$

Apply Eq.(3.86) and Eq.(3.69) to the numerator of Eq.(3.84) to obtain,

$$\begin{aligned} & \int_0^L EI(x) \left[\frac{\partial^2 X(x)}{\partial x^2} \right]^2 dx = \\ & \int_0^L E \left[\frac{1}{12} W \left(T_{ave-b}^3 - 3T_{ave-b}^2 \left(\frac{T_{ave-b} - T_{ave-t}}{L} \right) x + T_{ave-b} \left(\frac{T_{ave-b} - T_{ave-t}}{L} \right)^2 x^2 + \left(\frac{T_{ave-b} - T_{ave-t}}{L} \right)^3 x^3 \right) \right] \left[\frac{2}{L^2} \right]^2 dx \end{aligned} \quad (3.88)$$

After the integration and simplification, the above equation becomes,

$$\int_0^L EI(x) \left[\frac{\partial^2 X(x)}{\partial x^2} \right]^2 dx = \frac{EW}{3L^3} \left[T_{ave-b}^3 - \frac{3}{2} T_{ave-b}^2 (T_{ave-b} - T_{ave-t}) + \frac{1}{3} T_{ave-b} (T_{ave-b} - T_{ave-t})^2 + \frac{1}{4} (T_{ave-b} - T_{ave-t})^3 \right] \quad (3.89)$$

Apply Eq.(3.87), Eq.(3.85), and Eq.(3.66) to denominator of Eq.(3.84) to obtain,

$$\int_0^L \rho A(x) [X(x)]^2 dx + m [X(l_m)]^2 = \int_0^L \rho W \left(T_{ave-b} - \frac{T_{ave-b} - T_{ave-t}}{L} x \right) \left(\frac{x}{L} \right)^4 dx + m \left(\frac{l_m}{L} \right)^4 \quad (3.90)$$

After integration and simplification, the above equation becomes,

$$\int_0^L \rho A(x) [X(x)]^2 dx + m [X(l_m)]^2 = \rho WL \left[\frac{1}{5} T_{ave-b} - \frac{1}{6} (T_{ave-b} - T_{ave-t}) \right] + m \left(\frac{l_m}{L} \right)^4 \quad (3.91)$$

Substitution of Eq.(3.91) and Eq.(3.89) into Eq.(3.84) allows,

$$\omega^2 = \frac{\frac{EW}{3L^3} \left[T_{ave-b}^3 - \frac{3}{2} T_{ave-b}^2 (T_{ave-b} - T_{ave-t}) + \frac{1}{3} T_{ave-b} (T_{ave-b} - T_{ave-t})^2 + \frac{1}{4} (T_{ave-b} - T_{ave-t})^3 \right]}{\rho WL \left[\frac{1}{5} T_{ave-b} - \frac{1}{6} (T_{ave-b} - T_{ave-t}) \right] + m \left(\frac{l_m}{L} \right)^4} \quad (3.92)$$

Simplify above equation to obtain the final form,

$$\omega = \sqrt{\frac{EWL \left[T_{ave-b}^3 - \frac{3}{2} T_{ave-b}^2 (T_{ave-b} - T_{ave-t}) + \frac{1}{3} T_{ave-b} (T_{ave-b} - T_{ave-t})^2 + \frac{1}{4} (T_{ave-b} - T_{ave-t})^3 \right]}{3\rho WL^5 \left[\frac{1}{5} T_{ave-b} - \frac{1}{6} (T_{ave-b} - T_{ave-t}) \right] + 3ml_m^4}} \quad (3.93)$$

Eq.(3.93) is the fundamental frequency equation derived by Rayleigh method for the tapered beam with concentrated mass.

3.1.7 Rayleigh-Ritz Method

The Rayleigh-Ritz method is an extension of the Rayleigh's method with several important improvements. In addition to increased accuracy for estimating the fundamental frequency, the Rayleigh-Ritz method furnishes the capability to estimate higher natural frequencies and determine the associated mode shapes [1]. Like Rayleigh's method, the mode shape is assumed a priori. However, in Rayleigh-Ritz method, the mode shape is given in the form of an infinite series as shown below.

$$X(x) = \sum_{i=1}^n a_i f_i(x) \quad (3.94)$$

As the number of terms in infinite series approximation increases, more accurate results can be achieved.

Consider the Rayleigh quotient for tapered beam derived previously Eq.(3.84),

$$\omega^2 = \lambda_R = \frac{\int_0^L EI(x) \left[\frac{\partial^2 X(x)}{\partial x^2} \right]^2 dx}{\int_0^L \rho A(x) [X(x)]^2 dx + m [X(l_m)]^2}$$

The idea behind the Rayleigh-Ritz method is to minimize the frequency or Rayleigh quotient with respect to a_i 's. Then,

$$\frac{\partial \lambda_R}{\partial a_i} = \frac{\partial}{\partial a_i} \left[\frac{\int_0^L EI(x) \left[\frac{\partial^2 X(x)}{\partial x^2} \right]^2 dx}{\int_0^L \rho A(x) [X(x)]^2 dx + m [X(l_m)]^2} \right] = 0 \quad (3.95)$$

which yields,

$$\frac{\left\{ \begin{aligned} & \left[\int_0^L \rho A(x) [X(x)]^2 dx + m [X(l_m)]^2 \right] \frac{\partial}{\partial a_i} \left[\int_0^L EI(x) \left[\frac{\partial^2 X(x)}{\partial x^2} \right]^2 dx \right] \\ & - \left[\int_0^L EI(x) \left[\frac{\partial^2 X(x)}{\partial x^2} \right]^2 dx \right] \frac{\partial}{\partial a_i} \left[\int_0^L \rho A(x) [X(x)]^2 dx + m [X(l_m)]^2 \right] \end{aligned} \right\}}{\left[\int_0^L \rho A(x) [X(x)]^2 dx + m [X(l_m)]^2 \right]^2} = 0 \quad (3.96)$$

In order for the above equation to be valid, the denominator cannot be zero, then,

$$\begin{aligned} & \left[\int_0^L \rho A(x) [X(x)]^2 dx + m [X(l_m)]^2 \right] \frac{\partial}{\partial a_i} \left[\int_0^L EI(x) \left[\frac{\partial^2 X(x)}{\partial x^2} \right]^2 dx \right] \\ & - \left[\int_0^L EI(x) \left[\frac{\partial^2 X(x)}{\partial x^2} \right]^2 dx \right] \frac{\partial}{\partial a_i} \left[\int_0^L \rho A(x) [X(x)]^2 dx + m [X(l_m)]^2 \right] = 0 \end{aligned} \quad (3.97)$$

Rearrange this equation,

$$\frac{\partial}{\partial a_i} \left[\int_0^L EI(x) \left[\frac{\partial^2 X(x)}{\partial x^2} \right]^2 dx \right] - \frac{\left[\int_0^L EI(x) \left[\frac{\partial^2 X(x)}{\partial x^2} \right]^2 dx \right]}{\left[\int_0^L \rho A(x) [X(x)]^2 dx + m [X(l_m)]^2 \right]} \frac{\partial}{\partial a_i} \left[\int_0^L \rho A(x) [X(x)]^2 dx + m [X(l_m)]^2 \right] = 0 \quad (3.98)$$

Apply Eq.(3.84) to the above equation,

$$\frac{\partial}{\partial a_i} \left[\int_0^L EI(x) \left[\frac{\partial^2 X(x)}{\partial x^2} \right]^2 dx \right] - \omega^2 \frac{\partial}{\partial a_i} \left[\int_0^L \rho A(x) [X(x)]^2 dx + m [X(l_m)]^2 \right] = 0 \quad (3.99)$$

Simplify above equation to obtain,

$$\frac{\partial}{\partial a_i} \left[\int_0^L EI(x) \left[\frac{\partial^2 X(x)}{\partial x^2} \right]^2 dx - \omega^2 \left[\int_0^L \rho A(x) [X(x)]^2 dx + m [X(l_m)]^2 \right] \right] = 0 \quad (3.100)$$

Eq.(3.100) is the Rayleigh-Ritz equation for the tapered beam with a concentrated mass.

Apply Eq.(3.94) to the above equation,

$$\sum_{i=1}^n \frac{\partial}{\partial a_i} \left[\int_0^L EI(x) [a_i f_i'(x)]^2 dx - \omega^2 \left[\int_0^L \rho A(x) [a_i f_i(x)]^2 dx + m [a_i f_i(l_m)]^2 \right] \right] = 0 \quad (3.101)$$

The above equation can be written as,

$$\sum_{i=1, j=1}^n \frac{\partial}{\partial a_i} \left[\int_0^L EI(x) [a_i f_i'(x)] [a_j f_j''(x)] dx - \omega^2 \left[\int_0^L \rho A(x) [a_i f_i(x)] [a_j f_j(x)] dx + m [a_i f_i(l_m)] [a_j f_j(l_m)] \right] \right] = 0 \quad (3.102)$$

Stiffness matrix of the beam for transverse motion is given as,

$$k_y = \int EI(x) f_i'(x) f_j''(x) dx \quad (3.103)$$

Mass matrix of the beam can be expressed as,

$$m_y = \int \rho A(x) f_i(x) f_j(x) dx \quad (3.104)$$

Eq.(3.102) can be written in simpler form using Eq.(3.103) and Eq.(3.104).

$$\sum_{i=1, j=1}^n \frac{\partial}{\partial a_i} \left[a_i k_y a_j - \omega^2 [a_i m_y a_j + m [a_i f_i(x)] [a_j f_j(x)]] \right] = 0 \quad (3.105)$$

Performing a partial derivative with respect to a_i and obtain,

$$\sum_{j=1}^n \left[2k_y a_j - \omega^2 [2m_y a_j + 2m f_i(l_m) a_j f_j(l_m)] \right] = 0 \quad (3.106)$$

By rearranging above equation,

$$\sum_{j=1}^n 2 \left[k_y - \omega^2 [m_y + m f_i(l_m) f_j(l_m)] \right] a_j = 0 \quad (3.107)$$

In matrix form,

$$2 \left[[k] - \omega^2 \left[[m] + m \{f(l_m)\} \{f(l_m)\}^T \right] \right] \{a\} = \{0\} \quad (3.108)$$

Note that the mass matrix $[m]$ and the concentrated mass m is not the same.

In order for the above equation to be true, the determinant of coefficient matrix must vanish. Then,

$$\det \left[[k] - \omega^2 \left[[m] + m \{f(l_m)\} \{f(l_m)\}^T \right] \right] = 0 \quad (3.109)$$

or,

$$\det [[k] - \omega^2 [M]] = 0 \quad (3.110)$$

where, $[M]$ is the total mass matrix.

Assume the deflection function to be,

$$X(x) = a_1 x^2 + a_2 x^3 \quad (3.111)$$

Since the assumed deflection function has two terms, estimate of two natural frequencies can be obtained. From the equation above, two Ritz deflection functions can be obtained,

$$f_1 = x^2 \quad (3.112)$$

$$f_2 = x^3 \quad (3.113)$$

Then, the second derivatives of Ritz function is,

$$f_1'' = 2 \quad (3.114)$$

$$f_2'' = 6x \quad (3.115)$$

Mass matrix can be determined by Eq.(3.104),

$$m_{11} = \rho W \int_0^L \left(T_{ave-b} - \frac{T_{ave-b} - T_{ave-t}}{L} x \right) x^4 dx \quad (3.116)$$

$$m_{12} = m_{21} = \rho W \int_0^L \left(T_{ave-b} - \frac{T_{ave-b} - T_{ave-t}}{L} x \right) x^5 dx \quad (3.117)$$

$$m_{22} = \rho W \int_0^L \left(T_{ave-b} - \frac{T_{ave-b} - T_{ave-t}}{L} x \right) x^6 dx \quad (3.118)$$

Integration of above equations yields,

$$m_{11} = \frac{\rho WL^5 (T_{ave-b} - 5T_{ave-t})}{30} \quad (3.119)$$

$$m_{12} = m_{21} = \frac{\rho WL^6 (T_{ave-b} - 6T_{ave-t})}{42} \quad (3.120)$$

$$m_{22} = \frac{\rho WL^7 (T_{ave-b} - 7T_{ave-t})}{56} \quad (3.121)$$

Considering the concentrated mass, the total mass matrix can be written as,

$$M_{11} = \frac{\rho WL^5 (T_{ave-b} - 5T_{ave-t})}{30} + ml_m^4 \quad (3.122)$$

$$M_{12} = M_{21} = \frac{\rho WL^6 (T_{ave-b} - 6T_{ave-t})}{42} + ml_m^5 \quad (3.123)$$

$$M_{22} = \frac{\rho WL^7 (T_{ave-b} - 7T_{ave-t})}{56} + ml_m^6 \quad (3.124)$$

Stiffness matrix can be obtained by Eq.(3.103),

$$k_{11} = \frac{1}{3} WE \int_0^L \left(T_{ave-b}^3 - 3T_{ave-b}^2 \left(\frac{T_{ave-b} - T_{ave-t}}{L} \right) x + T_{ave-b} \left(\frac{T_{ave-b} - T_{ave-t}}{L} \right)^2 x^2 + \left(\frac{T_{ave-b} - T_{ave-t}}{L} \right)^3 x^3 \right) dx \quad (3.125)$$

$$k_{12} = k_{21} = WE \int_0^L \left(T_{ave-b}^3 - 3T_{ave-b}^2 \left(\frac{T_{ave-b} - T_{ave-t}}{L} \right) x + T_{ave-b} \left(\frac{T_{ave-b} - T_{ave-t}}{L} \right)^2 x^2 + \left(\frac{T_{ave-b} - T_{ave-t}}{L} \right)^3 x^3 \right) x dx \quad (3.126)$$

$$k_{22} = 3WE \int_0^L \left(T_{ave-b}^3 - 3T_{ave-b}^2 \left(\frac{T_{ave-b} - T_{ave-t}}{L} \right) x + T_{ave-b} \left(\frac{T_{ave-b} - T_{ave-t}}{L} \right)^2 x^2 + \left(\frac{T_{ave-b} - T_{ave-t}}{L} \right)^3 x^3 \right) x^2 dx \quad (3.127)$$

Integration of above equations allows,

$$k_{11} = \frac{EWL (T_{ave-t} + T_{ave-b}) (T_{ave-b}^2 - T_{ave-t}^2)}{12} \quad (3.128)$$

$$k_{12} = k_{21} = \frac{EWL^2 (T_{ave-b}^3 + 2T_{ave-b}^2 T_{ave-t} + 3T_{ave-b} T_{ave-t}^2 + 4T_{ave-t}^3)}{20} \quad (3.129)$$

$$k_{22} = \frac{EWL^3 (T_{ave-b}^3 + 3T_{ave-b}^2 T_{ave-t} + 6T_{ave-b} T_{ave-t}^2 + 10T_{ave-t}^3)}{20} \quad (3.130)$$

Combine stiffness and total mass matrices using Eq.(3.110) allows,

$$\det \begin{bmatrix} k_{11} - \omega^2 M_{11} & k_{12} - \omega^2 M_{12} \\ k_{21} - \omega^2 M_{21} & k_{22} - \omega^2 M_{22} \end{bmatrix} = 0 \quad (3.131)$$

The above determinant can be expanded as,

$$V\omega^4 + Z\omega^2 + Y = 0 \quad (3.132)$$

where,

$$V = (M_{11}M_{22} - M_{12}M_{21}) \quad (3.133)$$

$$Z = (k_{12}M_{21} + k_{21}M_{12} - k_{11}M_{22} - k_{22}M_{11})$$

$$Y = (k_{11}k_{22} - k_{21}k_{12}) \quad (3.134)$$

The equations shown above, Eq.(3.132) to Eq.(3.134), are the frequency equations for the tapered beam with a concentrated mass, derived by Rayleigh-Ritz method. The frequency equations have four roots,

$$\pm \frac{\sqrt{-2V(Z - \sqrt{Z^2 - 4VY})}}{2V} \quad (3.135)$$

and,

$$\pm \frac{\sqrt{-2V(Z + \sqrt{Z^2 - 4VY})}}{2V} \quad (3.136)$$

When the above root equations are evaluated, two roots will result in positive real numbers. Those two numbers are the first two fundamental frequencies of the tapered beam with concentrated mass.

3.1.8 Two Dimensional Plate Method

All the methods presented previously are the one-dimensional analysis and no considerations are given to the torsional vibration of the beam. This is often critical when the real figure to be represented as an analysis model has a wide width and/or a thin thickness, as in the case of this thesis [12]. Therefore, the main focus of this section is to model the blade as a thin plate and analyze its vibration behavior. The flat plate model is shown below in Figure 3.3.

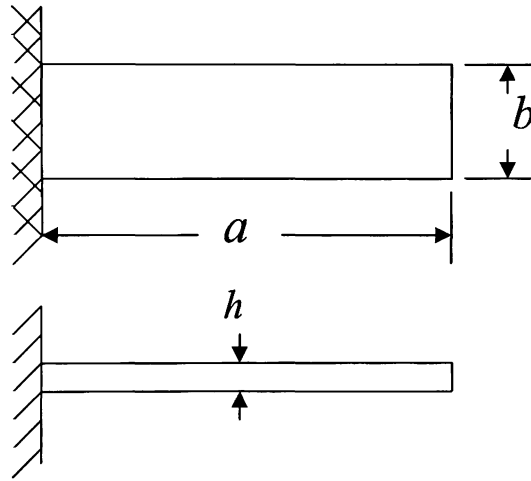


Figure 3.5: Two-dimensional flat plate model

The equation of motion of a flat plate based on Kirchhoff theory is,

$$D\nabla^4 w + \rho h w_{tt} = 0 \quad (3.137)$$

where, subscript indicates partial derivatives and ∇^4 is the biharmonic operator, $w(x, y; t)$ is the displacement and D is the flexural rigidity of the plate as defined by,

$$D = \frac{Eh^3}{12(1-\nu^2)} \quad (3.138)$$

where, h is the constant thickness of the plate and ν is the Poisson's ratio. By definition, the biharmonic operator or ∇^4 is,

$$\nabla^4 w = w_{xxxx} + 2w_{xyxy} + w_{yyyy} \quad (3.139)$$

The natural boundary conditions of a flat plate can be written as,

$$w_{xxx} + (2-\nu)w_{yyx} = 0 \quad (3.140)$$

$$w_{xx} + \nu w_{yy} = 0 \quad (3.141)$$

The geometric boundary conditions for a cantilever plate are,

$$w(0, y) = 0 \quad (3.142)$$

$$w_x(a, y) = w_y(a, y) = 0 \quad (3.143)$$

$$w_x(x, 0) = w_y(x, 0) = 0 \quad (3.144)$$

$$w_x(x, b) = w_y(x, b) = 0 \quad (3.145)$$

Assuming the solution to be harmonic in time,

$$w(x, y; t) = W(x, y) \cos(\omega t - \alpha) \quad (3.146)$$

Then, the Eq.(3.137) becomes,

$$\nabla^2 W - \lambda^4 W = 0 \quad (3.147)$$

This is the eigenvalue equation and λ is the eigenvalue. Where,

$$\lambda^4 = \frac{\omega^2 a^4 \rho h}{D} \quad (3.148)$$

Eigenvalue can also be written as,

$$\lambda^2 = \omega a^2 \sqrt{\frac{\rho h}{D}} \quad (3.149)$$

Since there is no closed form solution for this problem with given boundary conditions, the numerical computation must be performed to find the eigenvalue. The eigenvalue must be determined for various Poisson's ratio and length-width ratio ($\frac{a}{b}$). The table below shows the lists of eigenvalues for Poisson's ratio of 0.342 (titanium alloy).

Mode Sequence (n)								
a/b	1	2	3	4	5	6	7	8
2	3.420	14.50	21.28	47.32	59.76	91.24	92.68	117.7
2.5	3.406	17.58	21.24	56.14	59.72	104.3	117.1	143.4
3.0	3.395	20.68	21.20	59.60	65.07	117.3	118.0	183.7

Table 3.1: First eight eigenvalues (λ^2 's) for the vibration mode of the cantilever plate

Since there is an eigenvalue for each corresponding natural frequency, Eq.(3.149) is rewritten as,

$$\lambda_n^2 = \omega_n a^2 \sqrt{\frac{\rho h}{D}} \quad (3.150)$$

Rearrange above equation and obtain,

$$\omega_n = \frac{\lambda_n^2}{a^2} \sqrt{\frac{D}{\rho h}} \quad (3.151)$$

Substitute Eq.(3.138) into the above equation,

$$\omega_n = \frac{\lambda_n^2}{a^2} \sqrt{\frac{Eh^2}{12\rho(1-\nu^2)}} \quad (3.152)$$

The flat plate model does not include many of the real features of the blade, such as tapered thickness and concentrated mass. Although such simplifications are utilized, this equation can depict the torsional vibration and, therefore, is important to this thesis.

3.2 Finite Element Approach

Engineering analysis can be divided into two categories, classical methods and numerical methods [14]. Classical methods attempt to solve problems directly by forming governing differential equations based on the fundamental principles of physics. Classical methods can be sub-divided into two categories, exact method and approximate method. Exact solutions have closed form and can be obtained for simple problems, involving regular geometries, loading, and boundary conditions. The example of the exact method is the Bernoulli-Euler beam theory, which was presented previously. Classical approximate methods can be used for slightly more complex problem, but it still requires regular geometric shapes, simple boundary conditions, and well-defined loads. The example is the tapered beam with concentrated mass demonstrated previously using Rayleigh method and Rayleigh-Ritz method. Although classical methods may provide solutions that bear little resemblance to the real-life phenomena due to the limitation, they still provide a good insight of the problem.

Finite element analysis is a powerful numerical procedure that provides excellent approximation. Unlike the classical method, the finite element method is capable of solving complex problems. The finite element method uses the standard regular-shaped geometrical elements to approximate complex structural problems. Often, this is the only possible method to obtain solutions from complex problems, such as the one in this thesis.

3.2.1 Equation of Motion

The basic types of motion in a dynamic system are displacement u and the first and second derivatives of displacement with respect to time. These derivatives are velocity and acceleration given as,

$$\dot{u} = \frac{du}{dt} = V = \text{Velocity} \quad (3.153)$$

$$\ddot{u} = \frac{d^2u}{dt^2} = a = \text{Acceleration} \quad (3.154)$$

The simplest way to derive the equation of motion of dynamic system is to consider a single degree-of-freedom model shown below.

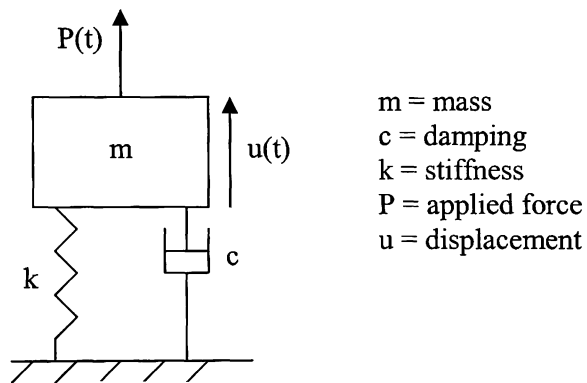


Figure 3.6: Single degree-of-freedom model

Newton's second law is applied to the model shown above. Summation of the force in vertical direction allows,

$$\uparrow \sum F = m\ddot{u} \quad (3.155)$$

$$P(t) - ku - c\dot{u} = m\ddot{u} \quad (3.156)$$

Rearranging the above equation,

$$m\ddot{u} + c\dot{u} + ku = P(t) \quad (3.157)$$

This is the equation of motion for the SDOF system. Similarly, the equation of motion for the multiple degree-of-freedom (MDOF) system can be expressed as,

$$[M]\{\ddot{u}\} + [c]\{\dot{u}\} + [k]\{u\} = \{P(t)\} \quad (3.158)$$

where,

$[M]$ is the mass matrix

$[k]$ is the stiffness matrix

$[c]$ is the damping coefficient matrix

3.2.2 Normal Modes Analysis

The equation of motion used for the normal modes analysis is the one of undamped free vibration, since the natural frequency of the system is not affected by loading or damping conditions [14]. Neglecting the damping and the applied force, the governing equation of motion becomes,

$$[M]\{\ddot{u}\} + [K]\{u\} = 0 \quad (3.159)$$

To solve an above equation, displacement vector is assumed a harmonic motion.

$$\{u\} = \{S\} \sin \omega t \quad (3.160)$$

where, $\{S\}$ is the eigenvector or mode shape and ω is the natural frequency.

Differentiation of the assumed harmonic solution above is,

$$\{\dot{u}\} = \{S\} \omega \sin t \omega t \quad (3.161)$$

$$\{\ddot{u}\} = -\{S\} \omega^2 \sin \omega t \quad (3.162)$$

Substituting above equations to the governing equation of motion allows,

$$-\omega^2[M]\{S\}\sin\omega t + [k]\{S\}\sin\omega t = 0 \quad (3.163)$$

Simplify above equation to obtain,

$$([k] - \omega^2[M])\{S\} = 0 \quad (3.164)$$

This equation is called the eigenvalue equation and ω^2 is the eigenvalue. For this equation to be true, $\{S\} \neq 0$ must also be true and the determinant of $([k] - \omega^2[M])$ must vanish.

$$\det([k] - \omega^2[M]) = 0 \quad (3.165)$$

This is the characteristic equation from which the eigenvalues or ω_n^2 can be obtained.

Corresponding to each eigenvector or mode shape $\{S\}$, there exists an eigenvalue that must satisfy the characteristic equation. Thus,

$$([k] - \omega_n^2[M])\{S_n\} = 0 \quad (3.166)$$

Each eigenvalue and eigenvector defines a vibration mode of the structure. The solution procedures and determination of the eigenvalues and mode shapes (eigenvector) using the finite element method is discussed in the next chapter. In addition, brief explanations of the eigenvalue extraction methods are presented in the Appendix.

Chapter 4

Finite Element Analysis Procedures

4.1 Finite Element Modeling Procedures

Finite Element Modeling (FEM) is one of the most important and probably the most difficult step of the analysis. It is essential to use FEM to solve complex and practical structural problems.. The modeling process includes the import of geometry from CAD program such as CATIA, geometric modification, meshing, examination of mesh, and element/material property definitions.

4.1.1 Importing Geometric Model into Finite Element Modeler

The blade geometry is transferred from CATIA workbench into MSC.PATRAN, one of the most reliable finite element modeling program available today. In order to import CATIA model into MSC.PATRAN, geometric model file of CATIA must be saved in transferable format, such as IGES (Initial Graphics Exchange Specifications). IGES is a neutral file format defined by ANSI for exchange of data across different CAD programs [8]. Although PATRAN accepts other formats, such as STEP, VDA, ACIS, and many other CAD program formats, IGES has been widely used in the professional industry to exchange data.. Therefore, it is the file format used in this thesis. CATIA model file can be easily converted to IGES file by “SAVE-AS” option of CATIA workbench. This converted file is imported into PATRAN by choosing the “File-Import” of PATRAN main menu. Extreme caution should be practice for the setting of global model tolerance. The global model tolerance sets a minimum distance between separate points, curves, surfaces, and solid. If entities are located within this tolerance from each

other, PATRAN sees the entities as one. On the other hands, the large tolerance may cause a gap between two connected entities. The selection of a proper global model tolerance is extremely critical, as one may observe. Therefore, it is generally a good engineering practice to utilize a 0.05 percent model tolerance with respect to the maximum size of the model. For this thesis, 0.05 percent model tolerance is approximately equivalent to 0.0021 m for the blade length of 4.137 m. The imported blade model is shown in Figure 4.1.

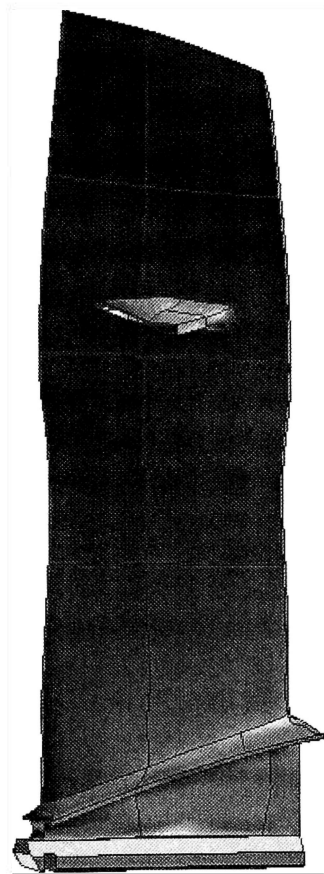


Figure 4.1 Imported blade model

4.1.2 Geometric Modification

In most cases, an imported geometric model requires modifications. Geometric models are not always prepared in CAD system with the consideration to analyze them later using finite element programs. Therefore, it must be modified to remove extraneous detail, to construct missing entities, and to reconstruct geometries for any distortion. IGES format is extremely broad standards that include many different types of geometric data and not all entity types in IGES are supported by PATRAN. This result in incomplete geometries, such as curves being translated as a series of points, or a regular solid being represented by its boundary surfaces. This model distortion must be repaired before any further actions can be performed. In the case of the blade model shown in Figure 4.1, each edge of the model must be matched with adjacent surfaces using “Edge-Match” function of PATRAN to close gaps between edges that opened during the importing process. In addition, PATRAN does not recognize the solid entities of IGES format. Therefore, solid model of the blade must be reformed by specifying the closed surfaces to form a boundary represented solid.

The blade model, shown in Figure 4.1, is not a topologically congruent model and, thus, it must be modified. Topological congruency is a prerequisite for creating a valid finite element model because it assures that all regions of the model geometry can be made into one connected entity during the element generation process. To be topologically congruent, the model must meet the following requirements.

- Adjacent regions of geometry share matching boundaries and vertices.
- The geometric components form a closed surface or solid region.

- There is no overlap between adjacent regions.

When edges of two adjacent regions are congruent, the same number of edge nodes will be created for each region at the boundary. This guarantees the formation of continuous elements along all boundaries of the model and no free-edges would be present.

In addition to ensuring the topological congruency, extra or unnecessary features of model must be removed for many reasons. The protruding shapes (two small attachments) at the mid-section of the blade must be removed and represented as a concentrated mass. This is done ,first to maintain the topological congruency, second to avoid concentration of mesh density, and third to eliminate small angles at small features. The bottom part of the blade is not necessary for the analysis and can be removed for simplification, since it is fixed to the fan/compressor rotor in the real case. The modified model of the blade is shown in Figure 4.2.

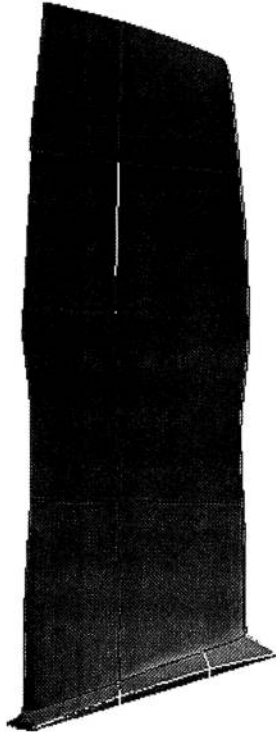


Figure 4.2: Modified blade model

4.1.3 Meshing of the Blade

The finite element method solves the problem by dividing the complex model into an assembled group of finite elements or small-interconnected pieces, commonly referred to as a mesh. The generation of meshes or “meshing” is performed semi-automatically using the “mesh” function of PATRAN. The solid model is generally subdivided into meshable sections and each section is carefully meshed using tetrahedron topology. The tetrahedron topology is utilized because of its conformability to complex shapes, although the computational speed may not be as fast as hexahedron topology. The mesh density must be chosen carefully to avoid the element overlapping and to avoid free-edges. The meshed finite element model is shown in Figure 4.3.

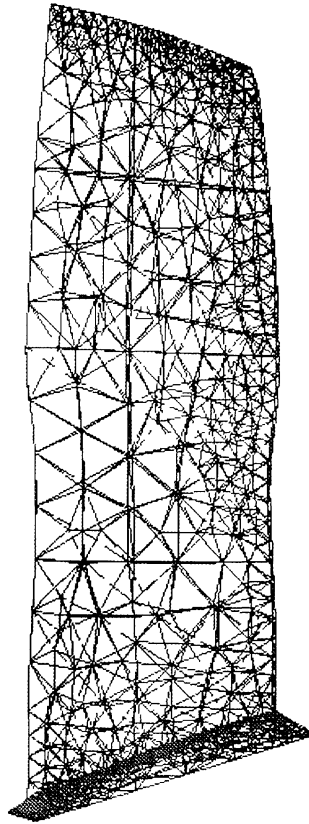


Figure 4.3: Meshed blade model

4.1.4 Blade Material Property, Element Property, and Constraint Definition

After completing the meshing process, the geometric property, material property, and the constraints for each element should be defined. Generally, the material property must be defined first. The fan blade is made of titanium alloy, as mentioned previously. In this thesis, SI unit is utilized throughout. Following material properties are supplied to PATRAN.

- Modulus of Elasticity (E) = 113.8 GPa
- Modulus of Rigidity (G) = 42.1 GPa
- Mass Density (ρ) = 4430 Kg/m³
- Poisson's Ratio (ν) = 0.342

The “Property” function of PATRAN defines the property of each mesh. The blade model consists of tetrahedron meshes and they must be defined as tetrahedron solid elements. Finally, load (if necessary) and boundary conditions must be applied to the model. For free vibration analysis, no loads are necessary. PATRAN has option of applying nodal constraints to geometric regions, instead of applying to each individual node. This is a useful function because some nodal constraints must be applied to certain regions or surfaces and it may not be practical to apply the boundary conditions to each single node. Since it is assumed that the blade is fixed to the fan/compressor rotor, any translations and rotations are constrained at the blade root.

4.1.5 Mesh Examination and Remeshing

After all the modeling processes are complete, the FE model must be examined for proper element symmetry and nodal connectivity to ensure the sound and accurate analysis results. The examination of mesh is generally performed in several different steps. The first step is to check the nodal connectivity of each element by visually observing the mesh for any free edges. The free edge is the portion of element that is not connected to adjacent elements. Although solver is capable of running an analysis of a model with free edges, resulting discontinuity of elements may cause an erroneous solution. Free edges and discontinuous nodes become clearly visible by using “Element-Verify” option of PATRAN. Then, the model must be equivalenced to join discontinuous nodes and to eliminate free edges. If free-edges can be eliminated, the meshing process was not successful and must be remeshed using different mesh sizes and density. In addition to the visual examination, the element shape test must be performed

using the PATRAN's automatic testing function. PATRAN checks each element for an aspect ratio, which is the maximum value of dimensional ratio of the opposing edges or faces. The aspect ratio implies the skewness of the elements. The shape of the element is extremely critical, since it is known that finite element analysis provides more accurate solutions when the aspect ratio is close to one. If too many elements in the model have high skewness and the aspect ratio is above the threshold value, then the model may have to be meshed for better shape and symmetry, using different mesh size and density.

4.2 Finite Element Analysis

After finite element modeling, the analysis file that contains finite element model data is submitted to the solver for the analysis. PATRAN has the capability of creating several format of analysis file that can be utilized by ABACUS, ANSYS, NASTRAN , and many other analysis codes [8]. The solver used for this thesis is MSC.NASTRAN 2001 Enterprise.

4.2.1 Creating Analysis File

First, PATRAN must create an analysis file called, "bulk data file." The bulk data file constraints all the information required for NASTRAN to perform an analysis. This file can be created by the "Analysis" option of PATRAN. Within this option, there is a sub-option called, "Solution type." Here, the solution type should be set to the "Normal Mode" for a modal analysis. In addition, the translation parameter must be set for NASTRAN to provide "xdb" file back. The bulk data file should appear as "jobname.bdf" in the same location where the model file is present.

4.2.2 Running Analysis

NASTRAN program is opened either using terminal commands or choosing PATRAN Windows icon. The bulk data file created by PATRAN is submitted to NASTRAN. After submitting an analysis file, NASTRAN begins analysis and, upon completion of the analysis, several output files including the one with xdb extension will be obtained. This xdb file contains all the results requested by PATRAN.

4.2.3 Importing and Obtaining Results

The xdb file must be imported to PATRAN to see a result. PATRAN reads xdb file when an option, “Analysis-Attach XDB,” is chosen. Then, solutions of modal analysis can be obtained by choosing, “Result” option. First ten natural frequencies will be listed in the result case box and the mode shapes can be observed graphically by choosing a desired mode from the box.

Chapter 5

Results

5.1 Analytical Solution

The analytical methods presented in this thesis are the Bernoulli-Euler beam method, Timoshenko beam theory, Rayleigh's method, Rayleigh-Ritz method, and two-dimensional flat plate method. First, following measurements are taken from the actual blade.

- Middle section width (W) = 0.1354 m
- Root-to-tip length of the blade at mid-section (L) = 0.3440 m
- Maximum thickness at the blade bottom ($T_{\max-b}$) = 0.0155 m
- Minimum thickness at the blade bottom ($T_{\min-b}$) = 0.0062 m
- Maximum thickness at the blade middle ($T_{\max-m}$) = 0.0073 m
- Minimum thickness at the blade middle ($T_{\min-m}$) = 0.0035 m
- Maximum thickness at the blade top ($T_{\max-t}$) = 0.0040 m
- Minimum thickness at the blade top ($T_{\min-t}$) = 0.0020 m
- Concentrated mass (m) = 0.05316 kg
- Distance to the concentrated mass from the blade root (l_m) = 0.22 m

Following material properties are given.

- Modulus of elasticity (E) = 113.8 GPa
- Modulus of Rigidity (G) = 42.1 GPa
- Mass density (ρ) = 4430 kg/m³

- Poisson's ratio (ν) = 0.342

5.1.1 Bernoulli-Euler Beam Method

In order to apply the Bernoulli-Euler method, the blade has been idealized as a cantilever beam with a uniform thickness throughout its length. First, it is necessary to calculate the average thickness at the blade root,

$$T_{ave-b} = \frac{T_{Max-b} + T_{Min-b}}{2} = \frac{0.0155 + 0.0062}{2} = 0.01085m$$

At the middle,

$$T_{ave-m} = \frac{T_{Max-m} + T_{Min-m}}{2} = \frac{0.0073 + 0.0035}{2} = 0.0054m$$

At the top,

$$T_{ave-t} = \frac{T_{Max-t} + T_{Min-t}}{2} = \frac{0.0040 + 0.0020}{2} = 0.0030m$$

Then, the average thickness of the blade is obtained as,

$$T_{ave} = \frac{T_{ave-b} + T_{ave-m} + T_{ave-t}}{3} = \frac{0.01085 + 0.0054 + 0.0030}{3} = 0.0064m$$

This value, $T_{ave} = 0.0064m$, has been used to represent the beam thickness. Therefore, the cross-sectional area of the beam is,

$$A = T_{ave}W = (0.0064)(0.1354) = 0.0008124m^2$$

The moment of inertia for rectangular beam is,

$$I = \frac{1}{12}WT_{ave}^3 = \frac{1}{12}(0.1354)(0.0064)^3 = 2.958 \times 10^{-9}m^4$$

Using the frequency equation, Eq.(3.49), determine first three natural frequencies,

$$\omega_n = \frac{(NL)_n^2}{L^2} \sqrt{\frac{EI}{\rho A}}$$

Where, eigenvalues are determined previously as $(NL)_1 = 1.8751$, $(NL)_2 = 4.6941$, and $(NL)_3 = 7.8548$. For first natural frequency,

$$\omega_1 = \frac{(NL)_1^2}{L^2} \sqrt{\frac{EI}{\rho A}} = \frac{1.8751^2}{0.344^2} \sqrt{\frac{(113.8 \times 10^9)(2.958 \times 10^{-9})}{(4430)(0.0008124)}} = 287.35 \frac{rad}{s}$$

$$F_1 = \frac{\omega_1}{2\pi} = \frac{287.35}{2\pi} = \boxed{45.73Hz}$$

Similarly,

$$\omega_2 = \frac{(NL)_2^2}{L^2} \sqrt{\frac{EI}{\rho A}} = \frac{4.6941^2}{0.344^2} \sqrt{\frac{(113.8 \times 10^9)(2.958 \times 10^{-9})}{(4430)(0.0008124)}} = 1800.82 \frac{rad}{s}$$

$$F_2 = \frac{\omega_2}{2\pi} = \frac{1800.82}{2\pi} = \boxed{286.61Hz}$$

Finally,

$$\omega_3 = \frac{(NL)_3^2}{L^2} \sqrt{\frac{EI}{\rho A}} = \frac{7.8548^2}{0.344^2} \sqrt{\frac{(113.8 \times 10^9)(2.958 \times 10^{-9})}{(4430)(0.0008124)}} = 5042.39 \frac{rad}{s}$$

$$F_3 = \frac{\omega_3}{2\pi} = \frac{5042.39}{2\pi} = \boxed{802.52Hz}$$

Mode	Frequency	Vibration Type
1	45.730 Hz	Transverse
2	286.61 Hz	Transverse
3	802.52 Hz	Transverse

Table 5.1: Summary of the Bernoulli-Euler solution

It should be noted that natural frequencies obtained are valid only for the transverse vibration, since there are no consideration given for torsional behavior of the beam. The concentrated mass is not considered in this analytical method. In addition, the averaged thickness of the beam is much smaller than the root thickness of the actual blade. This may alter the beam to be more flexible than the actual blade and result in lower natural frequencies. Nevertheless, the finite element solution should have a natural frequency close to that of the analytical solution obtained using the Bernoulli-Euler method.

5.1.2 Solution of the Timoshenko Beam Theory

The Timoshenko Beam theory is used to correct the Bernoulli-Euler solution for errors due to the rotary inertia and the shear deformation. In this thesis, the graphical approach was utilized. In order to utilize a graph shown in Figure 3.3, ratio of the radius of gyration to the length of beam must be determined first.

$$\sqrt{\frac{I}{AL^2}} = \sqrt{\frac{2.958 \times 10^{-9}}{(0.0008124)(0.344)^2}} = 0.0055$$

Since the ratio is very small, it is obvious that the effect of shear deformation and rotary inertia to the transverse vibration of the beam is negligible. This can be observed in Figure 3.3 that the correction factors are almost unity or equal to one. Therefore, Timoshenko beam theory proves that Bernoulli-Euler solution obtained in this thesis is accurate without the consideration of rotary inertia and shear deformation.

5.1.3 Solution of the Rayleigh's Method

Rayleigh's method can only be used to predict the fundamental frequency of the beam, but it is capable of analyzing more complex beam model. Unlike Bernoulli-Euler

method, it is an approximate method and the blade can be modeled as a tapered beam with concentrated mass. The calculation and results are shown below. First, the average thickness at the blade root and at the top of the blade must be determined.

$$T_{ave-b} = \frac{T_{Max-b} + T_{Min-b}}{2} = \frac{0.0155 + 0.0062}{2} = 0.01085m$$

$$T_{ave-t} = \frac{T_{Max-t} + T_{Min-t}}{2} = \frac{0.0040 + 0.0020}{2} = 0.0030m$$

Apply those values with geometric and material properties to Eq.(3.93),

$$\omega = \sqrt{\frac{EWL \left[T_{ave-b}^3 - \frac{3}{2} T_{ave-b}^2 (T_{ave-b} - T_{ave-t}) + \frac{1}{3} T_{ave-b} (T_{ave-b} - T_{ave-t})^2 + \frac{1}{4} (T_{ave-b} - T_{ave-t})^3 \right]}{3\rho WL^5 \left[\frac{1}{5} T_{ave-b} - \frac{1}{6} (T_{ave-b} - T_{ave-t}) \right] + 3ml_m^4}}$$

$$\omega = \sqrt{\frac{(113.8 \times 10^9)(0.1354)(0.344) \left[(0.01085)^3 - \frac{3}{2} (0.01085)^2 (0.01085 - 0.003) + \frac{1}{3} 0.01085 (0.01085 - 0.003)^2 + \frac{1}{4} (0.01085 - 0.003)^3 \right]}{3(4430)(0.1354)(0.344)^5 \left[\frac{1}{5} (0.01085) - \frac{1}{6} (0.01085 - 0.003) \right] + 3(0.05316)(0.22)^4}}$$

$$\omega = \sqrt{\frac{1245.14}{0.007843}} = 398.45 \frac{rad}{s}$$

$$F = \frac{\omega}{2\pi} = \frac{398.45}{2\pi} = \boxed{63.42Hz}$$

Mode	Natural Frequency	Vibration Type
1	63.420 Hz	Transverse

Table 5.2: Summary of the Rayleigh's method solution

As one may have noticed, the linear taper of the model assumed for this method may have resulted in "over-stiffened" analysis model. Since the thickness of the actual blade

exponentially tapers from root to tip (actual blade is thinner), the natural frequency obtained by Rayleigh's method is essentially higher than that of an actual blade. Although this may be the case, the finite element solution should have a fundamental natural frequency close to the one obtained using Rayleigh's method.

5.1.4 Rayleigh-Ritz Method

Rayleigh-Ritz method is considered as a one of the most reliable approximate method for the dynamic analysis of beams. Like Rayleigh's method, this method can handle more complex model, consisting of tapered beam and concentrated mass. The greatest advantage of this method over its predecessor is its capability to determine higher natural frequencies. The calculation for first two natural frequencies and its solution is shown below.

Four roots of the frequency equation are derived as,

$$\pm \frac{\sqrt{-2V(Z - \sqrt{Z^2 - 4VY})}}{2V} \quad \text{and} \quad \pm \frac{\sqrt{-2V(Z + \sqrt{Z^2 - 4VY})}}{2V}$$

where,

$$V = M_{11}M_{22} - M_{12}M_{21}$$

$$Z = k_{12}M_{21} + k_{21}M_{12} - k_{11}M_{22} - k_{22}M_{11}$$

$$Y = k_{11}k_{22} - k_{21}k_{12}$$

The total mass and stiffness matrices are given in Eq.(3.122) to Eq.(3.124) and Eq.(3.128) -Eq.(3.130) respectively as follows.

$$M_{11} = \frac{\rho WL^5 (T_{ave-b} - 5T_{ave-t})}{30} + ml_m^4$$

$$M_{12} = M_{21} = \frac{\rho WL^6 (T_{ave-b} - 6T_{ave-t})}{42} + ml_m^5$$

$$M_{22} = \frac{\rho WL^7 (T_{ave-b} - 7T_{ave-t})}{56} + ml_m^6$$

$$k_{11} = \frac{EWL(T_{ave-t} + T_{ave-b})(T_{ave-b}^2 - T_{ave-t}^2)}{12}$$

$$k_{12} = k_{21} = \frac{EWL^2 (T_{ave-b}^3 + 2T_{ave-b}^2 T_{ave-t} + 3T_{ave-b} T_{ave-t}^2 + 4T_{ave-t}^3)}{20}$$

$$k_{22} = \frac{EWL^3 (T_{ave-b}^3 + 3T_{ave-b}^2 T_{ave-t} + 6T_{ave-b} T_{ave-t}^2 + 10T_{ave-t}^3)}{20}$$

Since all the constants of stiffness and mass matrix are known, the above equations can be computed. The total mass matrix is determined as follows.

$$M_{11} = 0.002614269914$$

$$M_{12} = M_{21} = 0.0007101590714$$

$$M_{22} = 0.0002004974030$$

Now, the stiffness matrix must be determined.

$$k_{11} = 775.2497398$$

$$k_{12} = k_{21} = 217.3995520$$

$$k_{22} = 100.1297737$$

Determine the coefficients of the frequency equation,

$$V = 1.98284218 \times 10^{-7}$$

$$Z = -0.1084252864$$

$$Y = 30363.0158$$

Finally, roots of the frequency equation can be determined,

$$\pm \frac{\sqrt{-2(1.98284 \times 10^{-7})(-0.1084253) - \sqrt{(-0.1084253)^2 - 4(1.98284 \times 10^{-7})(30363.0158)}}}{2(1.982843 \times 10^{-7})}$$

and,

$$\pm \frac{\sqrt{-2(1.98284 \times 10^{-7})(-0.1084253) + \sqrt{(-0.1084253)^2 - 4(1.98284 \times 10^{-7})(30363.0158)}}}{2(1.982843 \times 10^{-7})}$$

The above root equations are evaluated as,

$$-2274.227, 2274.227, -544.199, 544.199$$

Taking only positive real roots, following solutions are obtained.

$$\omega_1 = 544.119 \frac{rad}{s}$$

$$f_1 = \frac{544.119}{2\pi} = \boxed{86.599 Hz}$$

$$\omega_2 = 2274.227 \frac{rad}{s}$$

$$f_1 = \frac{2274.227}{2\pi} = \boxed{361.95 Hz}$$

Mode	Natural Frequency	Vibration Type
1	86.599 Hz	Transverse
2	361.95 Hz	Transverse

Table 5.3: Summary of the Rayleigh-Ritz solution

The Rayleigh-Ritz solution did not match well with other solutions. This is due to the fact that only two terms are used in the infinite series to assume the mode shape. In

order to obtain more accurate solution, the number of terms in mode shape function must be increased.

5.1.5 Two-Dimensional Plate Method

So far, all the analytical solutions are obtained with an assumption that the blade can be represented as a beam and the torsional motion is negligible. While this assumption is valid for a slender object, the presence of torsional modes should not be neglected for many cases. Therefore, more accurate results can be obtained by considering the blade as a two-dimensional plate. Using Eq.(3.152), natural frequencies of the cantilever plate can be determined. The frequency equation is derived as,

$$\omega_n = \frac{\lambda_n^2}{a^2} \sqrt{\frac{Eh^2}{12\rho(1-\nu^2)}}$$

Consider that the plate has constant length, thickness, and width. Then,

$$a = L = 0.344m$$

$$h = T_{ave} = 0.0064m$$

Where, λ_n^2 is the eigenvalues that were determined previously and listed in Table 3.1. In order to find an eigenvalue for a particular plate geometry, the length-width (a/b) ratio must be known. The length-width ratio is found to be,

$$\frac{a}{b} = \frac{L}{W} = \frac{0.344}{0.1354} = 2.541 \cong 2.5$$

By observing, the Table 3.1 for λ_n^2 with $\frac{a}{b} = 2.5$, following λ_n^2 can be obtained.

$$\lambda_1^2 = 3.406 \quad \lambda_2^2 = 17.58 \quad \lambda_3^2 = 21.24 \quad \lambda_4^2 = 56.14$$

$$\lambda_5^2 = 59.72 \quad \lambda_6^2 = 104.3 \quad \lambda_7^2 = 117.1 \quad \lambda_8^2 = 143.4$$

Using all the values obtained, the natural frequencies can be determined.

$$\omega_1 = \frac{\lambda_1^2}{a^2} \sqrt{\frac{Eh^2}{12\rho(1-\nu^2)}} = \frac{3.406}{(0.344)^2} \sqrt{\frac{(113.8 \times 10^9)(0.0064)^2}{12(4430)(1-0.342^2)}} = 286.81 \frac{\text{rad}}{\text{s}}$$

$$F_1 = \frac{\omega_1}{2\pi} = \frac{286.81}{2\pi} = \boxed{45.65\text{Hz}}$$

$$F_2 = \left(\frac{\lambda_2^2}{\lambda_1^2}\right)(F_1) = \left(\frac{17.58}{3.406}\right)(45.65) = \boxed{235.61\text{Hz}}$$

$$F_3 = \left(\frac{\lambda_3^2}{\lambda_1^2}\right)(F_1) = \left(\frac{21.24}{3.406}\right)(45.65) = \boxed{284.66\text{Hz}}$$

$$F_4 = \left(\frac{\lambda_4^2}{\lambda_1^2}\right)(F_1) = \left(\frac{56.14}{3.406}\right)(45.65) = \boxed{752.39\text{Hz}}$$

$$F_5 = \left(\frac{\lambda_5^2}{\lambda_1^2}\right)(F_1) = \left(\frac{59.72}{3.406}\right)(45.65) = \boxed{800.37\text{Hz}}$$

$$F_6 = \left(\frac{\lambda_6^2}{\lambda_1^2}\right)(F_1) = \left(\frac{104.3}{3.406}\right)(45.65) = \boxed{1397.84\text{Hz}}$$

$$F_7 = \left(\frac{\lambda_7^2}{\lambda_1^2}\right)(F_1) = \left(\frac{117.1}{3.406}\right)(45.65) = \boxed{1569.39\text{Hz}}$$

$$F_8 = \left(\frac{\lambda_8^2}{\lambda_1^2}\right)(F_1) = \left(\frac{143.4}{3.406}\right)(45.65) = \boxed{1921.86\text{Hz}}$$

The summary of results is shown below.

Mode	Natural Frequency	Vibration Type (n,m)
1	45.650 Hz	1 st , Transverse (1,1)
2	235.61 Hz	1 st , Torsional (1,2)
3	284.66 Hz	2 nd , Transverse (2,1)
4	752.39 Hz	1 st , Transverse/Torsional (2,2)
5	800.37 Hz	3 rd , Transverse (3,1)
6	1397.8 Hz	2 nd , Transverse/Torsional (3,2)
7	1569.4 Hz	4 th , Transverse (4,1)
8	1921.9 Hz	3 rd , Transverse/Torsional (4,2)

Table 5.4: Summary of the analytical two-dimensional plate solution

As of Bernoulli-Euler method, this two-dimensional plate method uses a model having an averaged thickness at the root. In other words, the plate model is more flexible than the actual blade. Therefore, one can expect the result obtained by this method to be lower than that of the actual blade. Even if that is the case, valid finite element solution should still be similar to the analytical two-dimensional plate solution shown above.

5.2 Finite Element Solution

Finite element solutions are obtained for several different models that approximate the actual blade geometry. The first model is a straight plate with a concentrated mass. The next model is the tapered solid model with a concentrated mass. The last model is the actual blade model with concentrated mass.

5.2.1: Plate Finite Element Solution

The straight flat plate model is consisting of four-node quadrilateral plate elements (QUAD4) with material properties of titanium ($E= 113.8$ GPa, $G= 42.1$ GPa, $\nu= 0.342$, $\rho = 4430$ kg/m³) and a point mass element that represents the concentrated mass of 0.05316 kg is placed at 0.22 m from the bottom. Each of those QUAD4 plate elements has uniform thickness of 0.0064 m, length of 0.344 m, and width of 0.1354 m. Since the analytical plate methods presented previously uses the same model dimensions, solutions of the finite element plate method is close to the one obtained previously by the analytical plate method. In addition, the same dimensions are also used for the Bernoulli-Euler method. Therefore, this finite element plate model provides the result similar to the one obtained by Bernoulli-Euler method for the transverse vibration. Summary of the comparison is shown below.

Analytical Plate Solution			Plate FEA Solution		
Mode	Freq. (Hertz)	Vibration Type	Mode	Freq. (Hertz)	Vibration Type
1	45.650	1 st , transverse	1	42.457	1 st , transverse
2	235.61	1 st , torsional	2	216.68	1 st , torsional
3	284.66	2 nd , transverse	3	263.15	2 nd , transverse
4	752.39	1 st , transv/Torsion	4	684.50	1 st , transv/torsion
5	800.37	3 rd , transverse	5	734.38	3 rd , transverse
6	1397.8	2 nd , transv/Torsion	6	797.10	1 st , chordwise
7	1569.4	4 th , transverse	7	1247.4	2 nd , transv/torsion
8	1921.9	3 rd , transv/Torsion	8	1424.7	4 th , transverse

Table 5.5: Comparison between the analytical plate solution and the plate FEA solution

The table clearly reveals that the vibration behavior of the finite element plate is close to the analytical plate solution. For first to fifth modes of vibration, natural frequencies and the vibration types of the finite element plate resembles the one of analytical plate. The large difference can be observed in the sixth mode. One can observe that the sixth mode of finite element solution is the chordwise vibration mode that cannot be determined by analytical methods. In other words, the chordwise vibration mode is skipped in the case of the analytical plate method. Thus, the seventh mode of finite element plate and the sixth mode of analytical reference coincide as shown in the table. Consequently, the eighth mode of the plate is close to the seventh mode of analytical reference. The finite element plate solution is proven accurate and can be used for the comparison with the blade finite element solution.

5.2.2 Finite Element Solution of Tapered Solid Model

The tapered solid model consists of ten-nodes tetrahedron solid elements (TET10). Each of those solid elements is given the material properties of titanium alloy. Tapered thickness of this solid model varies linearly from 0.1085 m at the bottom to 0.003 m at the top. In addition, the point mass element represents the concentrated mass of 0.05316 kg placed at 0.22 m from the root. Since the same dimensions are used for the computation of approximate analytical solutions, the natural frequencies obtained from the finite element tapered solid model should be close to the one obtained from Rayleigh's method. This similarity should be valid only for the transverse vibration modes, since the approximate method neglects the presence of torsional vibration. Summary of the comparison is shown below.

Rayleigh's Method Solution			Tapered Solid FEA Solution		
Mode	Freq. (Hertz)	Vibration Type	Mode	Freq. (Hertz)	Vibration Type
1	63.420 Hz	1 st , transverse	1	61.855	1 st , transverse
2	N/A	N/A	2	258.74	1 st , torsional
3	N/A	N/A	3	278.34	2 nd , transverse
4	N/A	N/A	4	652.01	1 st , transv/torsion
5	N/A	N/A	5	692.08	3 rd , transverse
6	N/A	N/A	6	1056.6	1 st , chordwise
7	N/A	N/A	7	1283.8	2 nd , transv/torsion
8	N/A	N/A	8	1360.2	3 rd , transv/torsion

Table 5.6: Comparison between Rayleigh's method and the tapered solid FEA Solutions

Due to the limitation of Rayleigh's method, the comparison can be made only for the fundamental frequency. The table clearly reveals that the first natural frequency obtained using the Rayleigh's method is almost identical to the one obtained by the finite element method. Thus, the tapered solid solution is valid and can be used for the comparison with blade solution in the next section.

5.2.3 Finite Element Solution of the Blade Model

Finally, the blade model provides the most reliable and accurate solution. As mentioned previously, this model consists of ten-node tetrahedron solid elements that have material property of titanium alloy. Two protruding attachments of the actual blade are represented as a concentrated mass using a point mass element of 0.05316 kg. Since there is no analytical solution available to compare with the blade solution, other finite

element solutions that were proven previously would be used for the comparison. In the table below, comparisons are made with tapered solid model and plate model solutions to prove the validity of the blade model solution.

Plate FEA solution			Blade FEA solution		
Mode	Freq. (Hertz)	Vibration Type	Mode	Freq. (Hertz)	Vibration Type
1	42.457	1 st , transverse	1	47.685	1 st , transverse
2	216.68	1 st , torsional	2	227.98	2 nd , transverse
3	263.15	2 nd , transverse	3	296.67	1 st , torsional
4	684.50	1 st , transv/torsion	4	479.56	3 rd , transverse
5	734.38	3 rd , transverse	5	983.18	4 th , transverse
6	797.10	1 st , chordwise	6	1179.5	1 st , transv/torsion
7	1247.4	2 nd , transv/torsion	7	1585.8	2 nd , transv/torsion
8	1424.7	4 th , transverse	8	1660.4	3 rd , transv/torsion

Table 5.7: Comparison between the plate FEA and the blade FEA solutions

As one can observe from the table, the vibration behavior of the finite element blade is very similar to that of a plate model. Although the mode sequence is different, it is clearly visible that those two solutions share the close similarities. For instance, the first three vibration modes are almost the same, except that the second and the third modes are switched. The deviation of the blade solution from the plate solution is due to the twist of the actual blade. It is physically possible that the blade twist allows the chordwise vibration mode to appear as the transverse and/or torsional vibration modes.

As a proof, the chordwise vibration mode that is visible for the straight plate model is not observable in the case of twisted blade model. Next, the blade solution is compared with the tapered solid FEA solution in the table shown below.

Tapered Solid FEA solution			Blade FEA solution		
Mode	Freq. (Hertz)	Vibration Type	Mode	Freq. (Hertz)	Vibration Type
1	61.855	1 st , transverse	1	47.685	1 st , transverse
2	258.74	1 st , torsional	2	227.98	2 nd , transverse
3	278.34	2 nd , transverse	3	296.67	1 st , torsional
4	652.01	1 st , transv/torsion	4	479.56	3 rd , transverse
5	692.08	3 rd , transverse	5	983.18	4 th , transverse
6	1056.6	1 st , chordwise	6	1179.5	1 st , transv/torsion
7	1283.8	2 nd , transv/torsion	7	1585.8	2 nd , transv/torsion
8	1360.2	3 rd , transv/torsion	8	1660.4	3 rd , transv/torsion

Table 5.8: Comparison between the tapered solid FEA and the blade FEA solutions

One may observe from the table that the tapered solid solution shares the close similarity with the blade solution for the first three vibration modes. As in the case of the plate solution, the blade solution deviates away from the tapered solid solution for the higher modes due to the twist of an actual blade. Nevertheless, it is appropriate to state here that the finite element solution of the blade model is valid and accurate.

5.2.4 Close Examination of the Plate Finite Element Solution

MSC.Patran 2001 r2a 26-Jun-03 14:18:13

Fringe: SC1:DEFAULT, A1:Mode 1 : Freq. = 42.457: Eigenvectors, Translational-(NON-LAYERED) (MAG)

Deform: SC1:DEFAULT, A1:Mode 1 : Freq. = 42.457: Eigenvectors, Translational

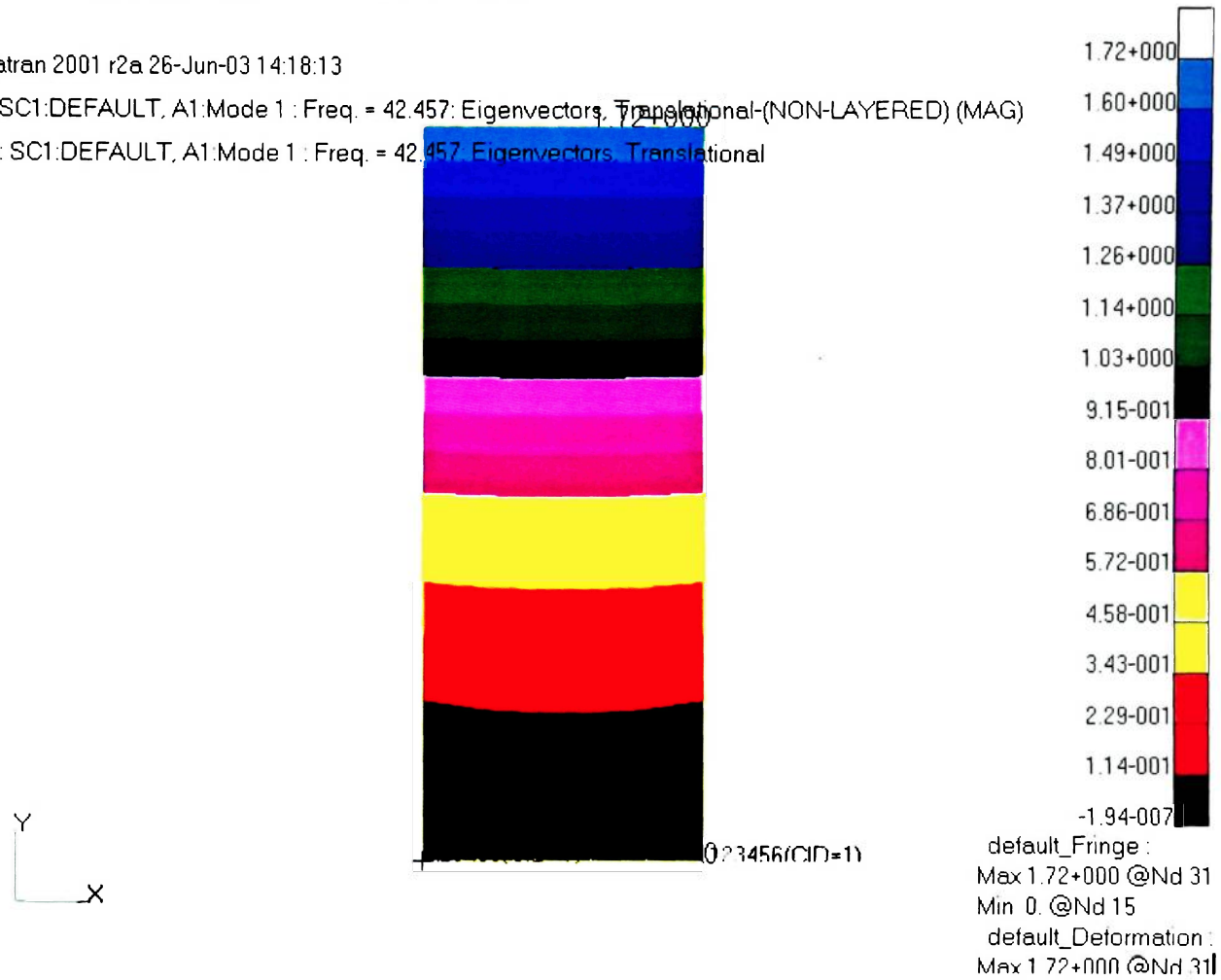


Figure 5.1: Mode 1 of the flat plate model

MSC.Patran 2001 r2a 26-Jun-03 14:18:25

Fringe: SC1:DEFAULT, A1:Mode 2 : Freq. = 216.68: Eigenvectors, Translational (NON-LAYERED) (MAG)

Deform: SC1:DEFAULT, A1:Mode 2 : Freq. = 216.68: Eigenvectors, Translational

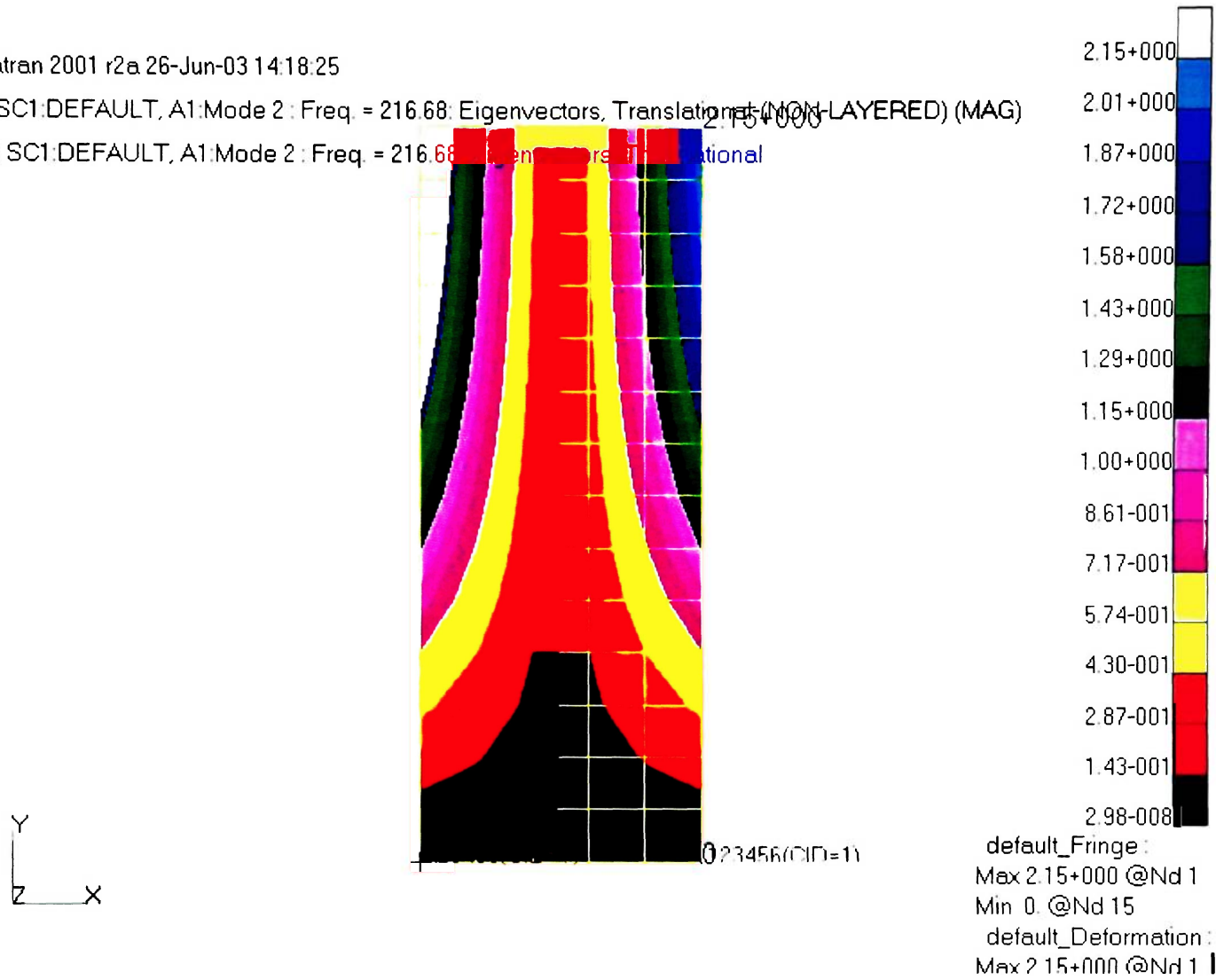


Figure 5.2: Mode 2 of the flat plate model

MSC.Patran 2001 r2a 26-Jun-03 14:18:48

Fringe: SC1:DEFAULT, A1:Mode 3 : Freq. = 263.15: Eigenvectors, Transitional (NON-LAYERED) (MAG)

Deform: SC1:DEFAULT, A1:Mode 3 : Freq. = 263.15: Eigenvectors, Transitional (NON-LAYERED) (MAG)

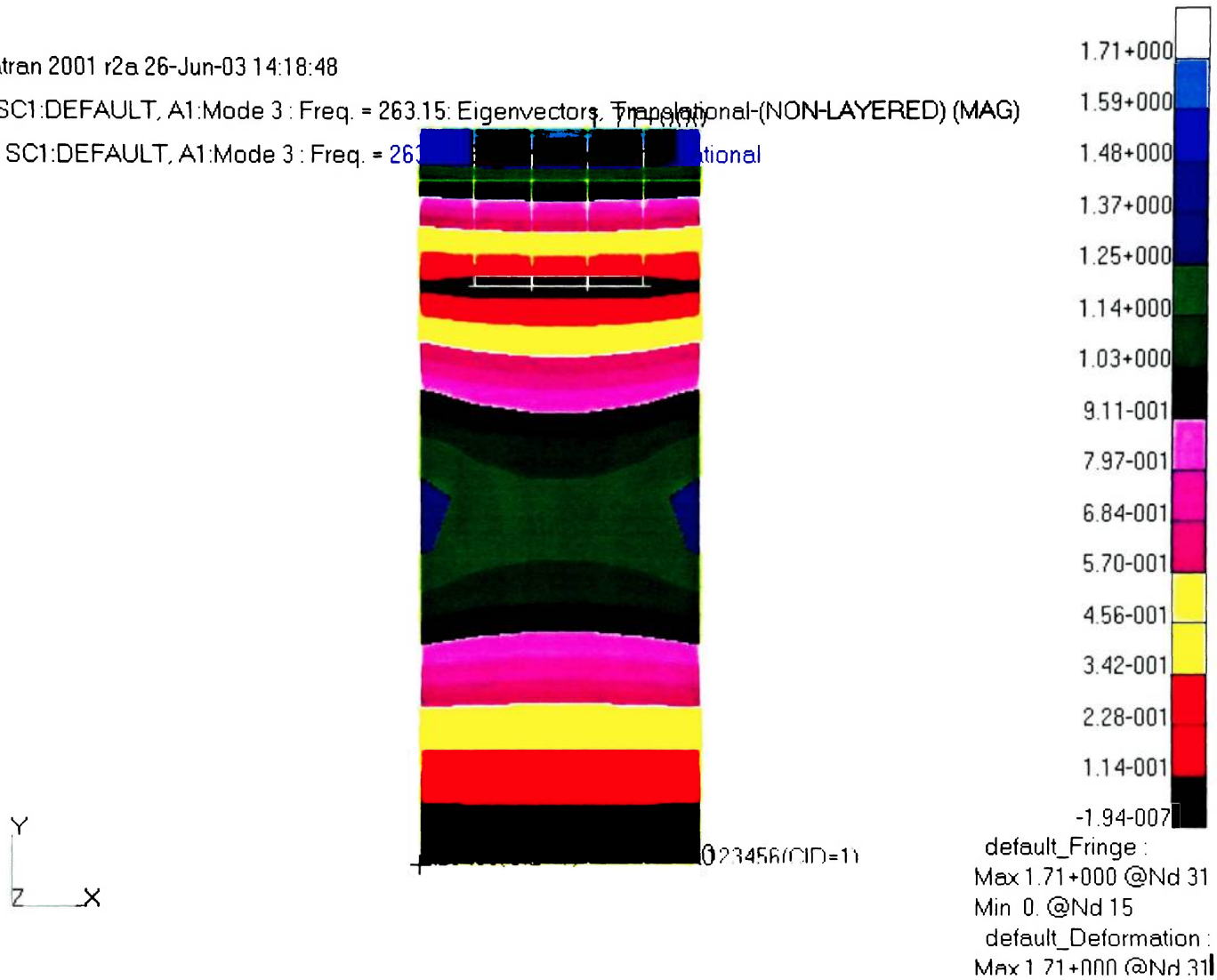
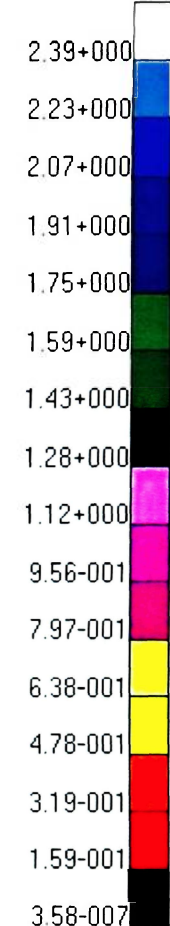
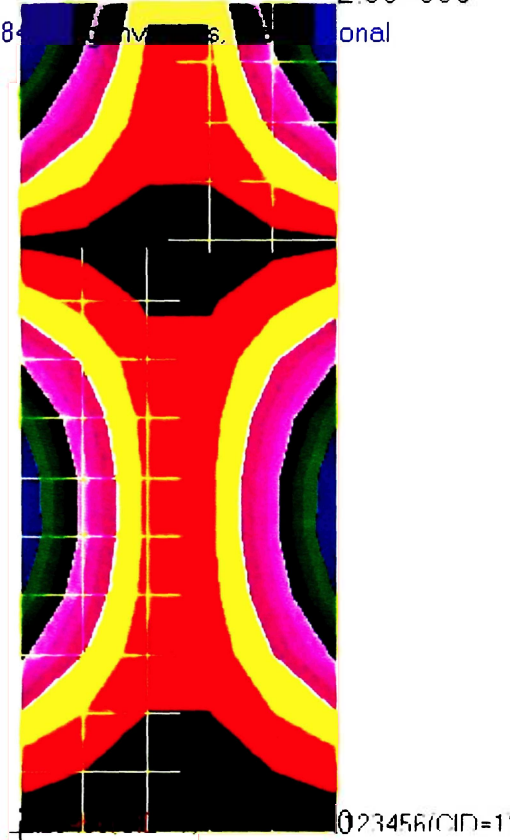


Figure 5.3: Mode 3 of the flat plate model

MSC.Patran 2001 r2a 26-Jun-03 14:19:12

Fringe: SC1:DEFAULT, A1:Mode 4: Freq. = 684.5; Eigenvectors, Translational (NON-LAYERED) (MAG)

Deform: SC1:DEFAULT, A1:Mode 4: Freq. = 684.5; Eigenvectors, Translational



default_Fringe :
Max 2.39+000 @Nd 1
Min 0. @Nd 15
default_Deformation :
Max 2.39+000 @Nd 1

Figure 5.4: Mode 4 of the flat plate model

MSC.Patran 2001 r2a 26-Jun-03 14:19:22

Fringe: SC1:DEFAULT, A1:Mode 5 : Freq. = 734.38: Eigenvectors, Translational-(NON-LAYERED) (MAG)

Deform: SC1:DEFAULT, A1:Mode 5 : Freq. = 734.38: Eigenvectors, Translational-(NON-LAYERED) (MAG)

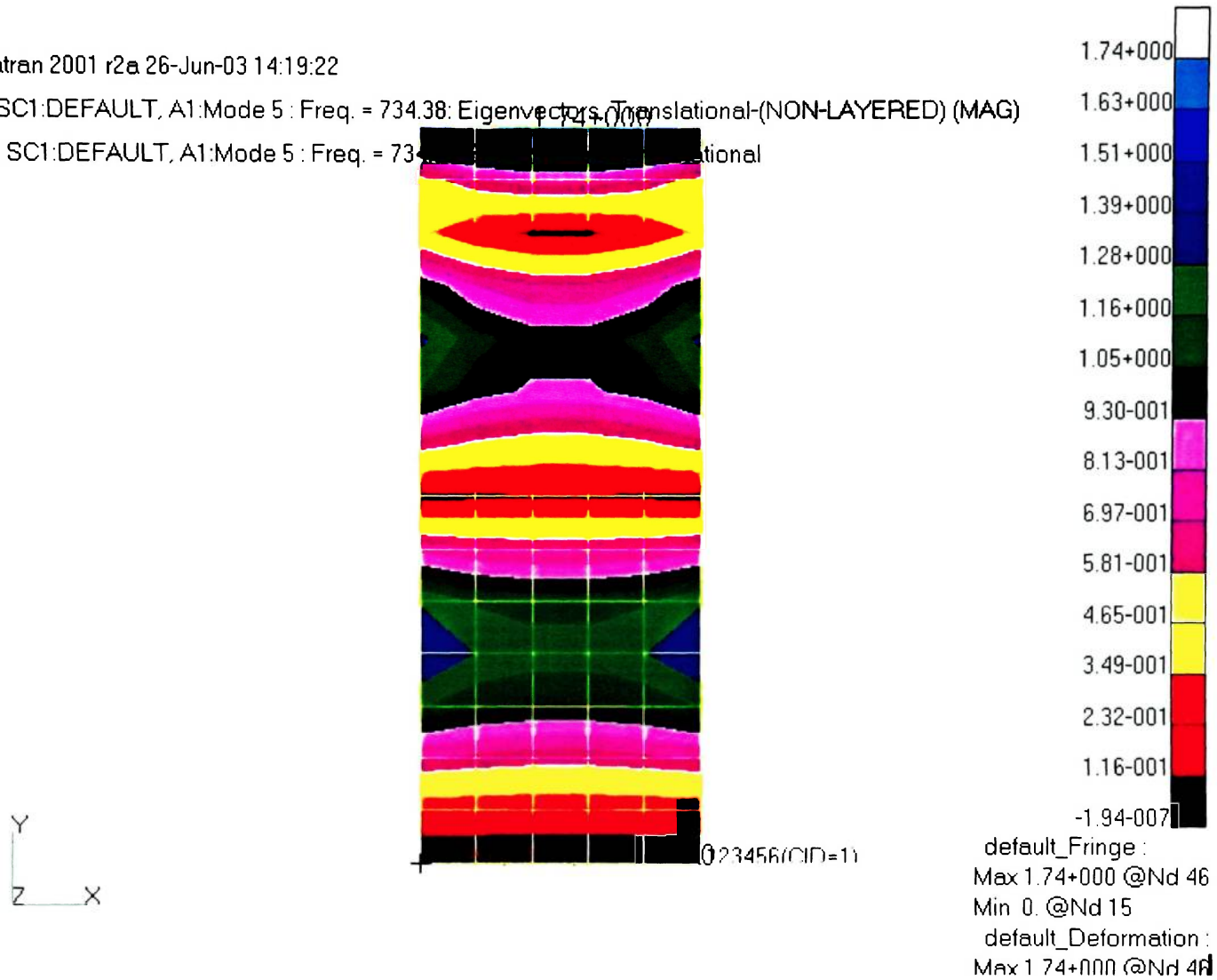


Figure 5.5: Mode 5 of the flat plate model

MSC.Patran 2001 r2a 26-Jun-03 14:19:34

Fringe: SC1:DEFAULT, A1:Mode 6 : Freq. = 797.1: Eigenvectors, Translational-(NON-LAYERED) (MAG)

Deform: SC1:DEFAULT, A1:Mode 6 : Freq. = 797.1: Eigenvectors, Translational (MAG)

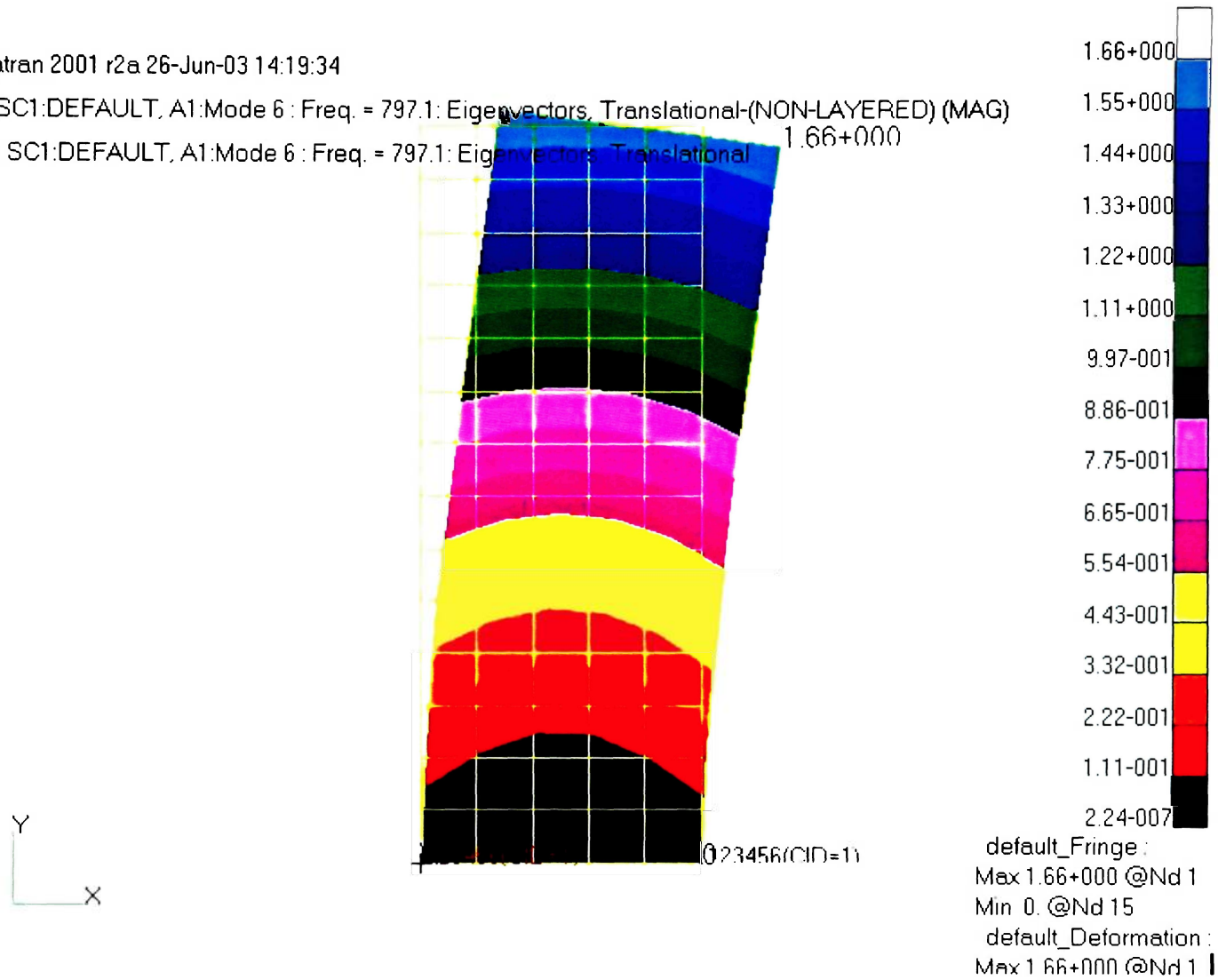


Figure 5.6: Mode 6 of the flat plate model

MSC.Patran 2001 r2a 26-Jun-03 14:19:46

Fringe: SC1:DEFAULT, A1:Mode 7 : Freq. = 1247.4; Eigenvectors, Translations (NON-LAYERED) (MAG)

Deform: SC1:DEFAULT, A1:Mode 7 : Freq. = 1247.4; Eigenvectors, Translations (NON-LAYERED) (MAG)

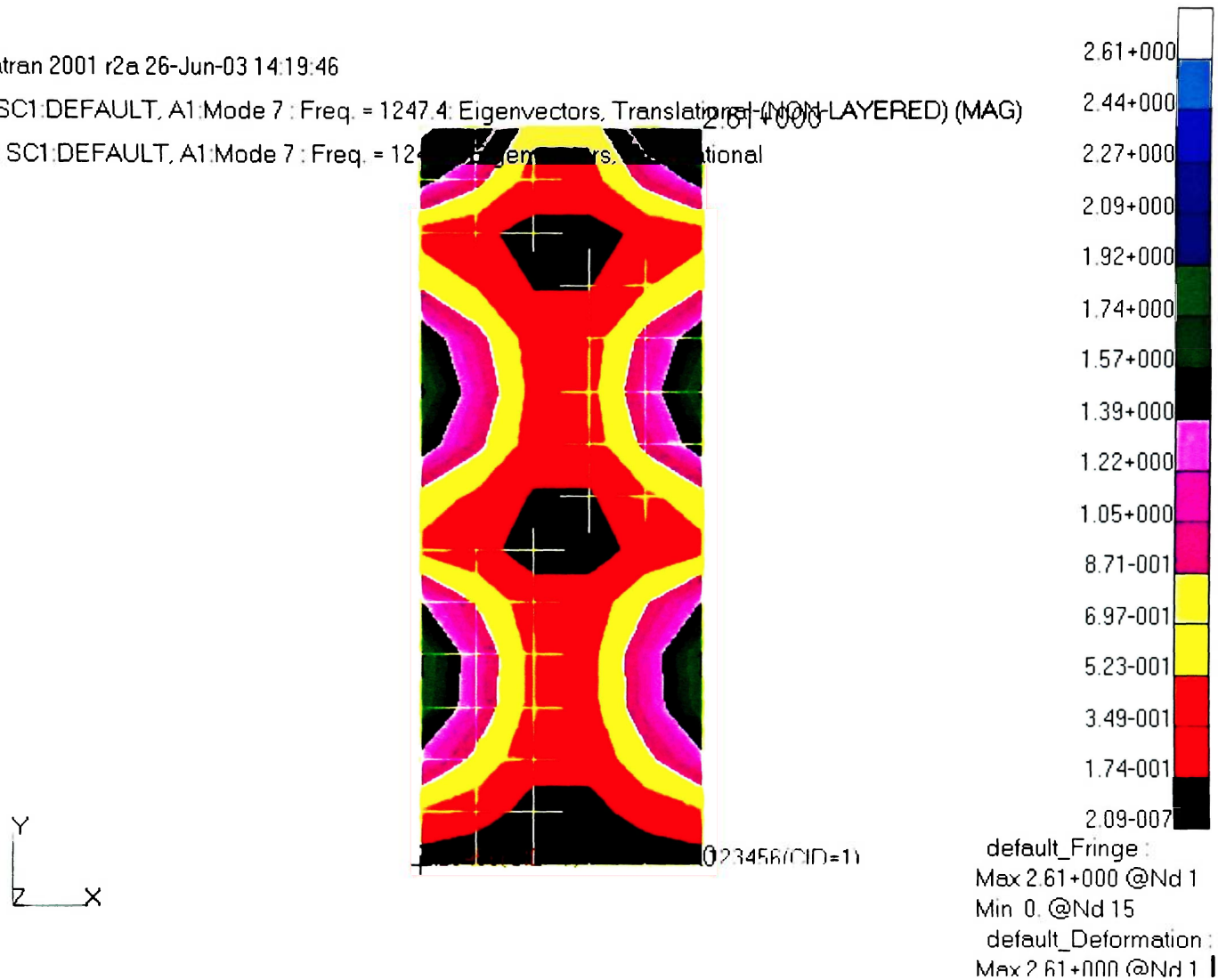


Figure 5.7: Mode 7 of the flat plate model

MSC.Patran 2001 r2a 26-Jun-03 14:19:55

Fringe: SC1:DEFAULT, A1:Mode 8 : Freq. = 1424.7: Eigenvectors, Translational-(NON-LAYERED) (MAG)

Deform: SC1:DEFAULT, A1:Mode 8 : Freq. = 1424.7: Eigenvectors, Translational

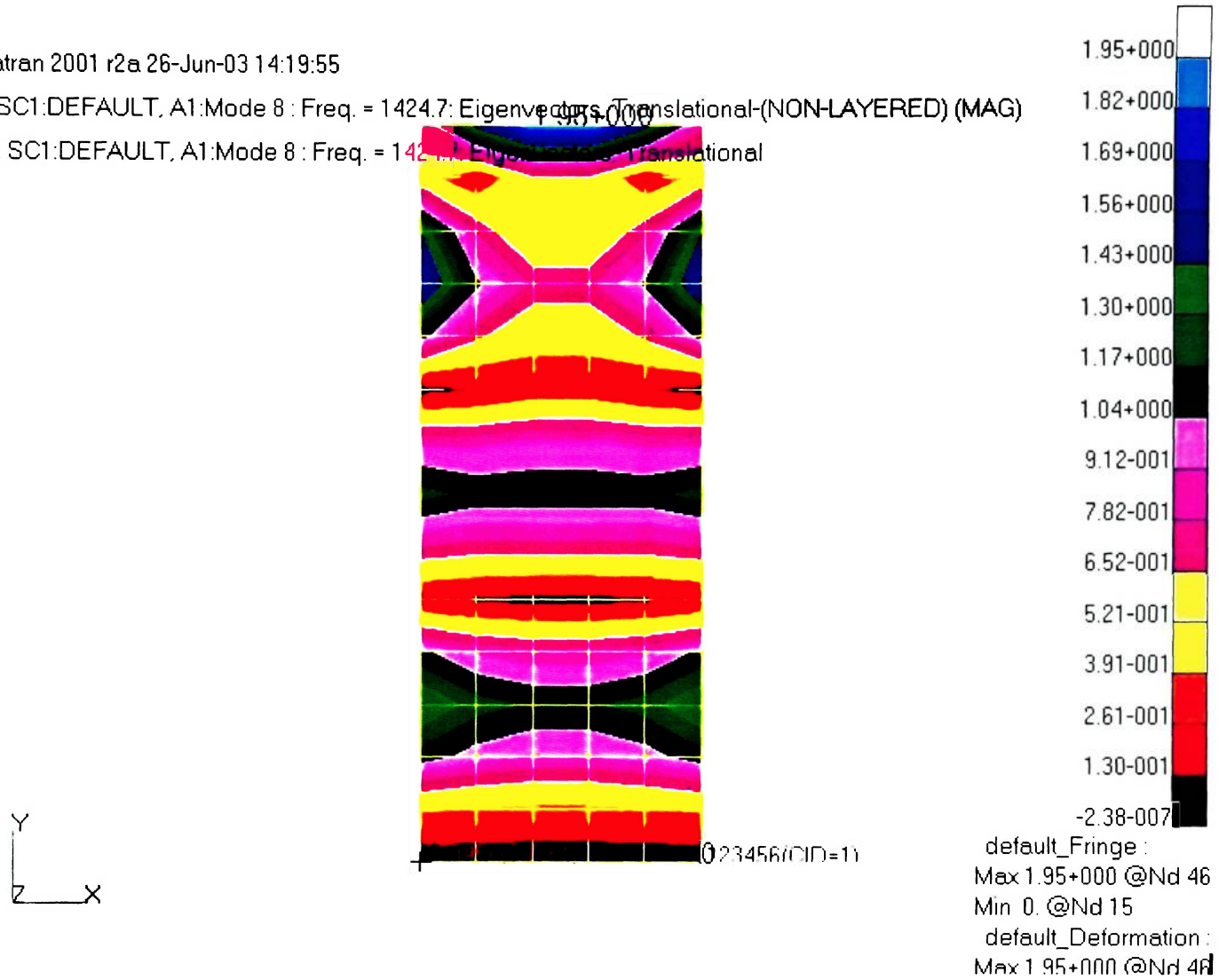


Figure 5.8: Mode 8 of the flat plate model

The first natural frequency of this model is 42.457 hertz and the mode shape is dominantly transverse as shown in Figure 5.1. No nodes are present for the first transverse mode, since there is no location where the mode shape intersects the zero displacement line. As one may notice, the value of natural frequency obtained from this finite element analysis is very close to the one obtained from Bernoulli-Euler method and analytical plate method as predicted previously.

The second natural frequency is found to be 216.68 hertz and the mode shape is dominantly torsional. Since it is the first torsional mode, the single node is present at the center of the plate along the length. The node location is ranging from 0.0542 m to 0.08138 m from either plate edges and it can be observed in Figure 5.2 as a single black line. The second natural frequency obtained from this analysis is similar to the one obtained from analytical plate method.

The third natural frequency is 263.15 hertz and the mode shape is dominantly transverse as shown in Figure 5.3. This natural frequency is similar to the one obtained from Bernoulli-Euler and analytical plate methods. One node can be seen as a single black line across the plate width at approximately two-third of the length from the plate bottom. The exact measurement shows that it is located approximately 0.2794 m from the bottom.

The fourth mode of vibration exhibits both transverse and torsional characteristics and the natural frequency is found to be 684.50 hertz. Two nodes can be observed in Figure 5.4 as a black line across the plate width and a dark red line along the plate length. Since it is the combination of second transverse and first torsional modes, it can also be interpreted in the two dimensional notation as $\omega_{2,1}$. The transverse node is located

approximately 0.254 m from the fixed bottom and the torsional node is ranging from 0.05425 m to 0.08138 m from either plate edge.

The fifth mode of vibration is dominantly transverse and its natural frequency is 734.38 hertz. It has two nodes as shown in Figure 5.5. The first node is located at 0.1778 m from the bottom and shown as a single black line across the plate width. The second one is located at 0.3048 m from the bottom and similarly shown as a black line.

The sixth mode of vibration has a characteristic of both chordwise (lateral) and transverse vibrations. Since the mode shape does not intersect the zero displacement line, no nodes are present. As mentioned previously, this vibration mode is not depicted in any analytical solutions due to the fact that consideration of chordwise motion is neglected for all the analytical method utilized in this thesis.

The seventh mode of vibration exhibits both transverse and torsional characteristics. The natural frequency is 1247.4 hertz and three nodes, two transverse and one torsional, are present. The first transverse node is located at approximately 0.1524 m to 0.1778 m from the plate bottom. The second transverse node is located at 0.2794 m to 0.3048 m from the bottom. The torsional node is located at the center along the plate length and ranging from 0.05425 m to 0.08138 m from either plate edge.

The eighth mode of vibration is dominantly transverse and has three nodes. The first node is located at 0.1270 m from the bottom and it is shown as a black line. The second node is at 0.2286 m and it can be seen as a red line with black spots. The third one is at 0.3302 m and it is shown as a yellow line with red spots.

Close Examination of the Tapered Solid Finite Element Solution

MSC.Patran 2001 r2a 17-May-03 20:05:49

Fringe: SC1:DEFAULT, A2:Mode 1 : Freq. = 61.855: Eigenvectors, Translational-(NON-LAYERED) (MAG)

Deform: SC1:DEFAULT, A2:Mode 1 : Freq. = 61.855: Eigenvectors, Translational

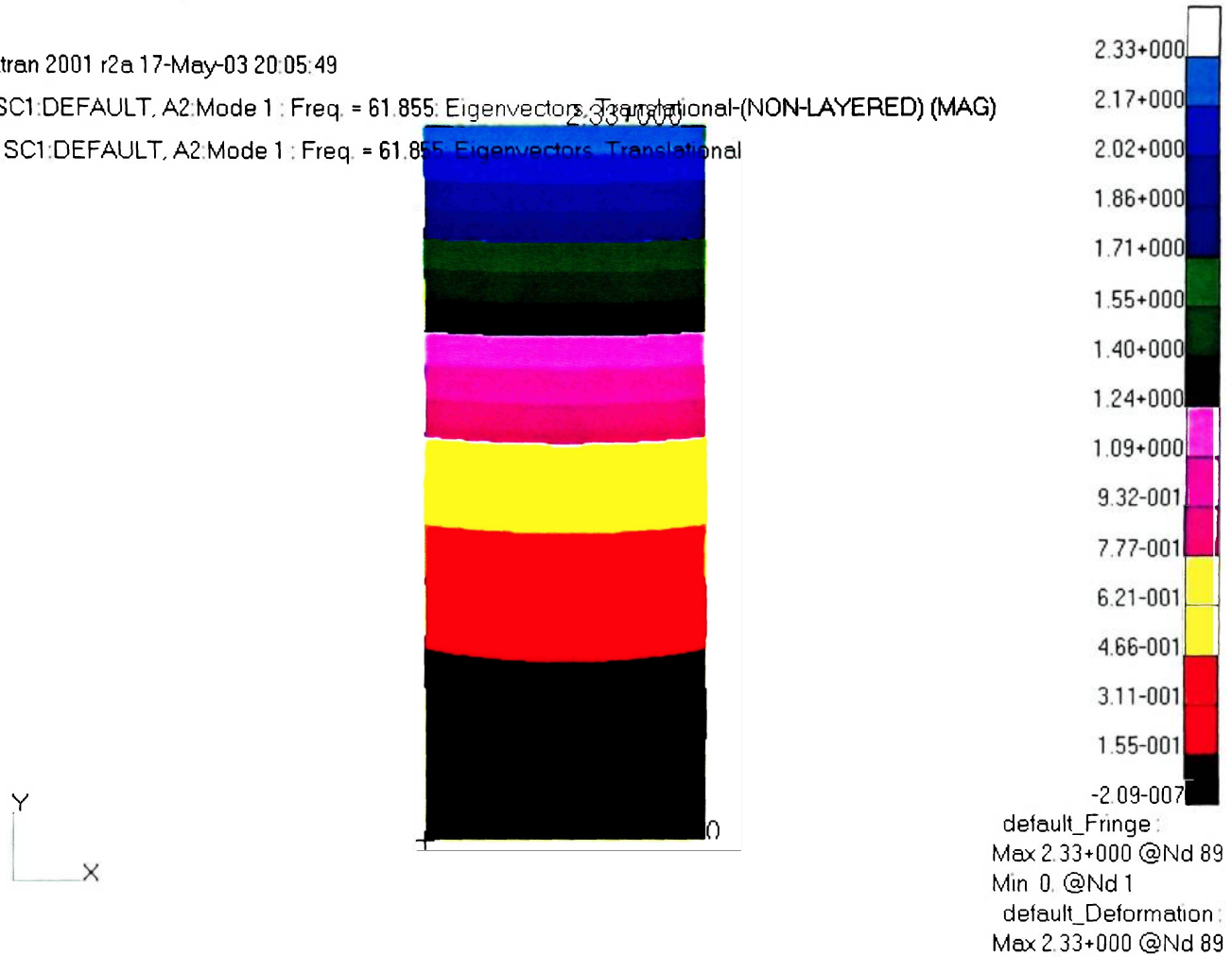


Figure 5.9: Mode 1 of the tapered solid model

MSC.Patran 2001 r2a 17-May-03 20:06:12

Fringe: SC1:DEFAULT, A2:Mode 2 : Freq. = 258.74 Eigenvalue, Translational-(NON-LAYERED) (MAG)

Deform: SC1:DEFAULT, A2:Mode 2 : Freq. = 258.74 Eigenvalue, Translational

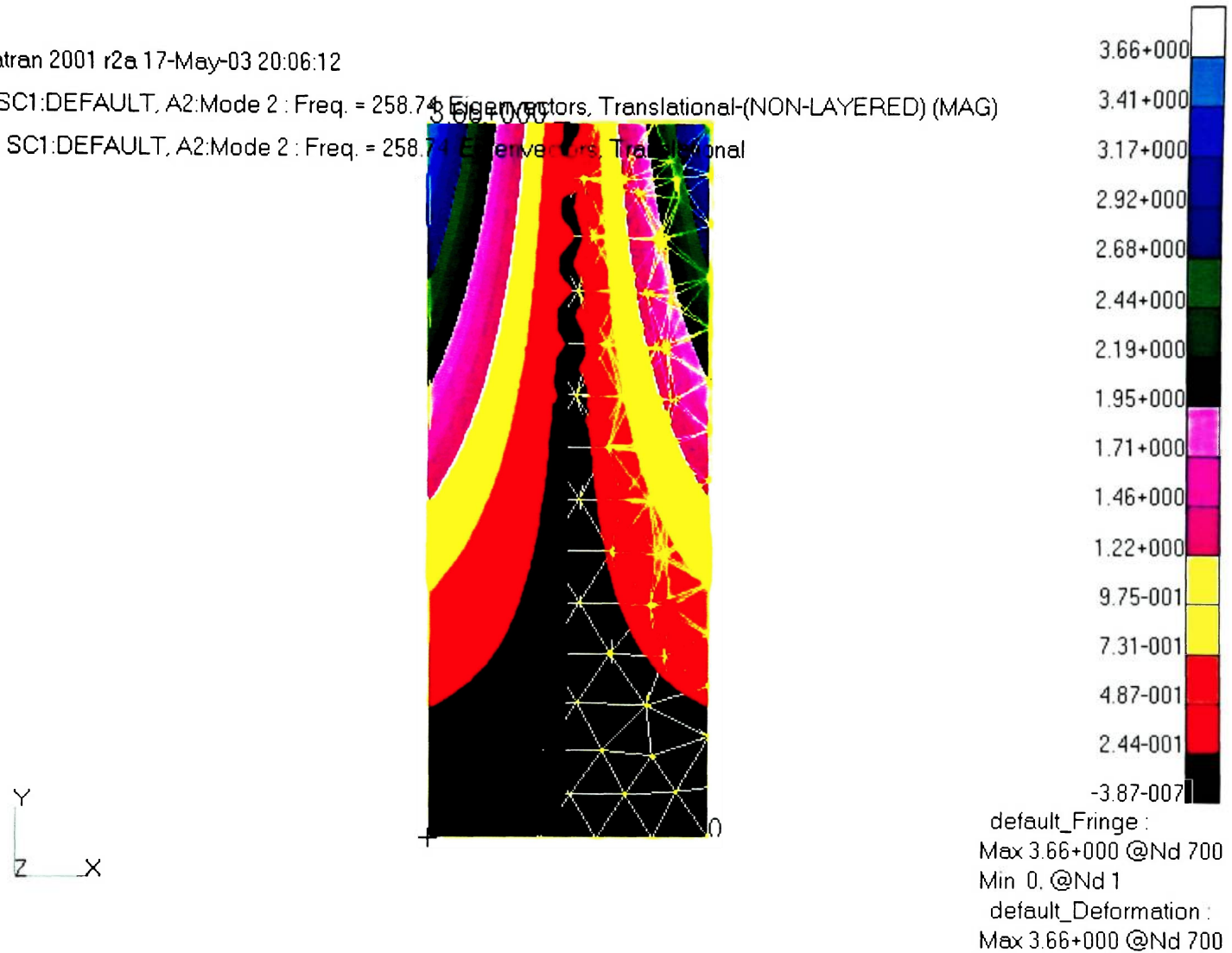


Figure 5.10: Mode 2 of the tapered solid model

MSC.Patran 2001 r2a 17-May-03 20:06:26

Fringe: SC1:DEFAULT, A2:Mode 3 : Freq. = 278.34: Eigenvectors, Translational-(NON-LAYERED) (MAG)

Deform: SC1:DEFAULT, A2:Mode 3 : Freq. = 278.34: Eigenvectors, Translational-(NON-LAYERED) (MAG)

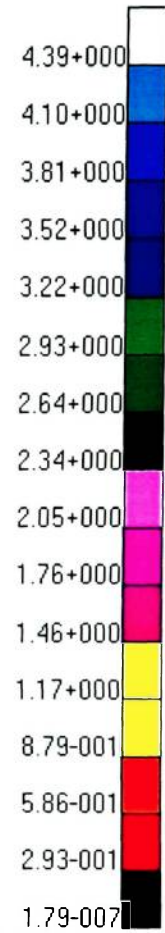
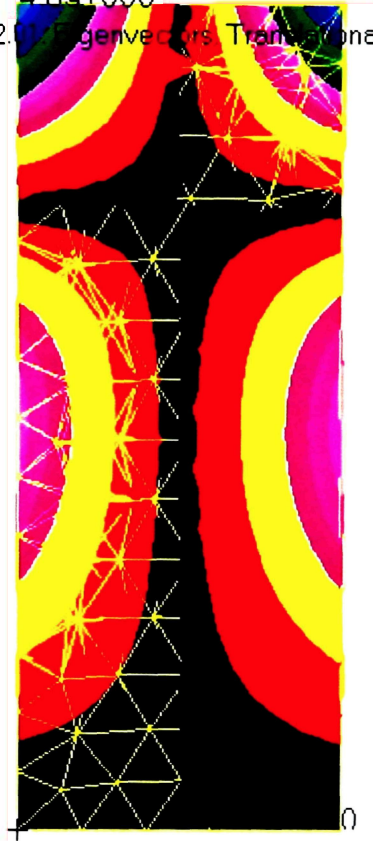
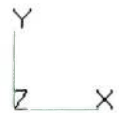


Figure 5.11: Mode 3 of the tapered solid model

MSC.Patran 2001 r2a 17-May-03 20:06:46

Fringe: SC1:DEFAULT, A2:Mode 4 : Freq. = 652.01 Eigenvectors, Translational-(NON-LAYERED) (MAG)

Deform: SC1:DEFAULT, A2:Mode 4 : Freq. = 652.01 Eigenvectors, Translational



default_Fringe :
Max 4.39+000 @Nd 700
Min 0. @Nd 1
default_Deformation :
Max 4.39+000 @Nd 700

Figure 5.12: Mode 4 of the tapered solid model

MSC.Patran 2001 r2a 17-May-03 20:07:05

Fringe: SC1:DEFAULT, A2:Mode 5 : Freq. = 692.08; Eigenvector 5: 3D rotational (NON-LAYERED) (MAG)

Deform: SC1:DEFAULT, A2:Mode 5 : Freq. = 692.08; Eigenvector 5: 3D rotational



Figure 5.13: Mode 5 of the tapered solid model

MSC.Patran 2001 r2a 17-May-03 20:07:20

Fringe: SC1:DEFAULT, A2:Mode 6 : Freq. = 1056.7: Eigenvectors, Translational-(NON-LAYERED) (MAG)

Deform: SC1:DEFAULT, A2:Mode 6 : Freq. = 1056.7: Eigenvectors, Translational

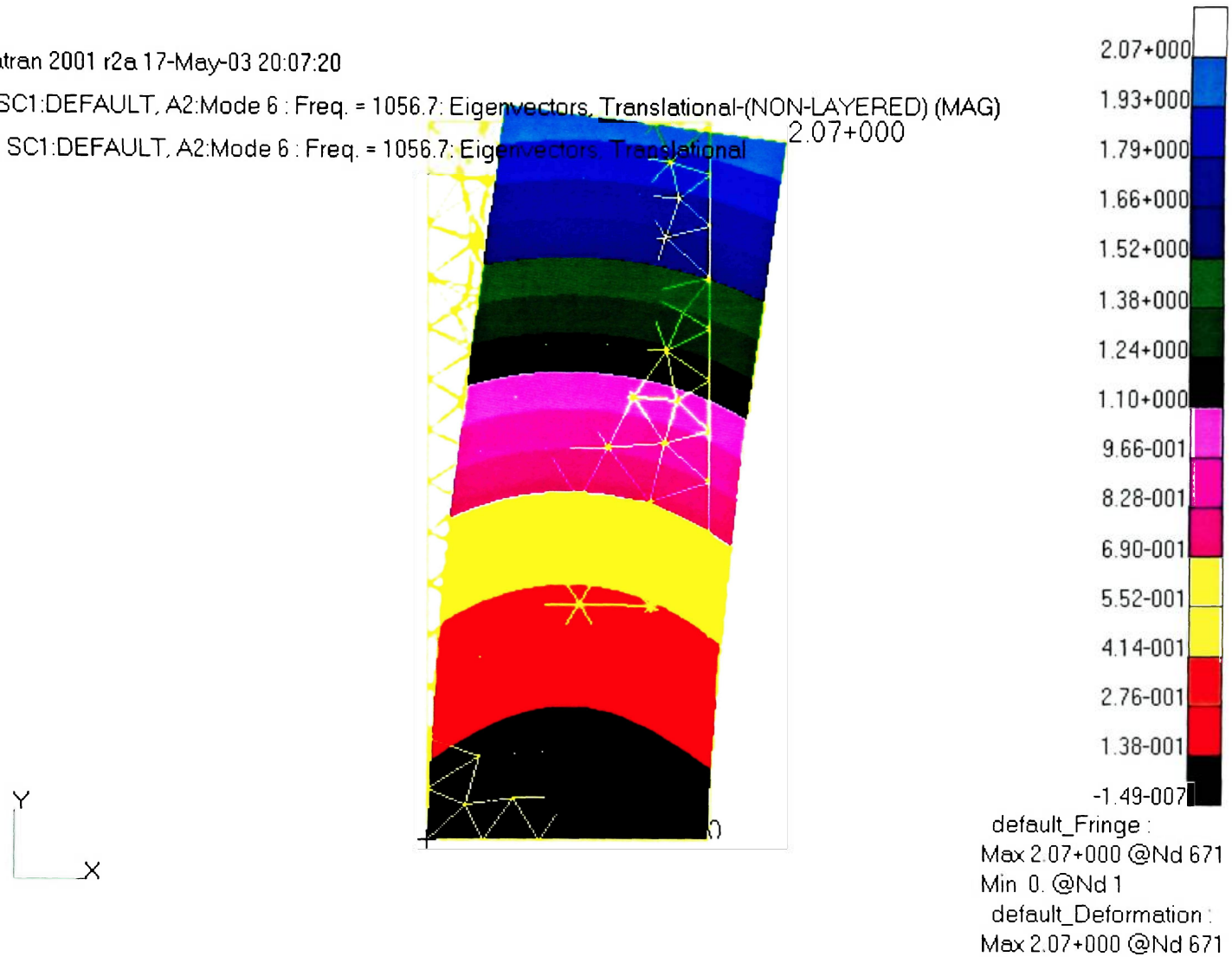
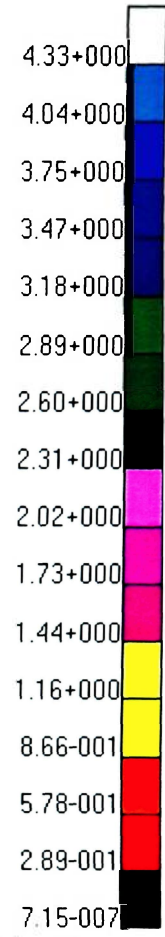
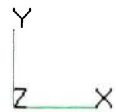


Figure 5.14: Mode 6 of the tapered solid model

MSC.Patran 2001 r2a 17-May-03 20:07:33

Fringe: SC1:DEFAULT, A2:Mode 7 : Freq. = 1283.8 Hz Eigenvectors, Translational-(NON-LAYERED) (MAG)

Deform: SC1:DEFAULT, A2:Mode 7 : Freq. = 1283.8 Hz Eigenvectors, Translational



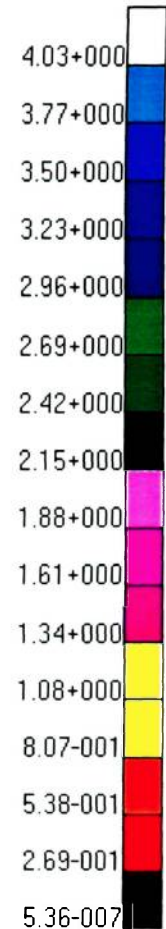
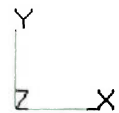
default_Fringe :
Max 4.33+000 @Nd 700
Min 0. @Nd 1
default_Deformation :
Max 4.33+000 @Nd 700

Figure 5.15: Mode 7 of the tapered solid model

MSC.Patran 2001 r2a 17-May-03 20:07:47

Fringe: SC1:DEFAULT, A2:Mode 8 : Freq. = 1360.2; Eigenvectors, Translational-(NON-LAYERED) (MAG)

Deform: SC1:DEFAULT, A2:Mode 8 : Freq. = 1360.2; Eigenvectors, Translational



default_Fringe :
Max 4.03+000 @Nd 89
Min 0. @Nd 1
default_Deformation :
Max 4.03+000 @Nd 89

Figure 5.16: Mode 8 of the tapered solid model

The first mode of vibration is dominantly transverse and the natural frequency is 61.855 hertz. It has no nodes as shown in Figure 5.9. As one can observe, the natural frequency is similar to the one obtained by Rayleigh method.

The second natural frequency is 258.74 hertz and the mode shape is dominantly torsional. It has a single node at the center of the model along the length shown as a lengthwise black line in Figure 5.10. This torsional node is located at approximately 0.0677 m from either edge of the model. Although Rayleigh and Rayleigh-Ritz methods do not provide any solutions for the torsional vibration and they cannot be used for a comparison, one can still observe that this torsional natural frequency is similar to that of the analytical plate method.

The third mode of vibration is dominantly transverse and has a single node. The transverse node is located at 0.2638 m from the root of the model. This node can be observed as a black line across the model width in Figure 5.11. The third natural frequency is 278.34 hertz.

The fourth vibration mode exhibits both transverse and torsional characteristics. It has two nodes where one of them is transverse and another one is torsional. The transverse node is located at approximately 0.2619 m from the fixed bottom shown as a chordwise black line in Figure 5.12. The torsional node is located at the center of the model along the length as a lengthwise black line. The measurement shows that this transverse node is located at approximately 0.0679 m from either edge. Those two nodes together appear on the model as a black “cross.” The fourth natural frequency is determined to be 652.01 hertz.

The fifth mode of vibration is dominantly transverse and the natural frequency is determined to be 692.08 hertz. Two nodes are present for this vibration mode, where the first node is located approximately 0.1882 m and the second one is located approximately 0.3029 m from the fixed bottom. Those nodes can be observed in Figure 5.13 as two black lines across the model width.

The sixth vibration mode is characterized with purely lateral vibration and has no node, as shown in Figure 5.14. The frequency is 1056.6 hertz and no analytical methods can depict this lateral vibration mode, as mentioned previously.

The seventh vibration mode exhibits both transverse and torsional vibration. The natural frequency is 1283.8 hertz and there are three nodes, two transverse and one torsional. The first transverse node is located at 0.1759 m and the second one is at 0.2949 m from the bottom. Those transverse nodes can be seen in Figure 5.15 as black lines across the model. Torsional node is located at the center of the model along the length and it can be seen as a lengthwise black line.

The eighth natural frequency is 1360.2 hertz and the mode shape exhibits both transverse and torsional vibration. The transverse node can be seen at approximately 0.1368 m from the bottom, as shown in Figure 5.16. The “point” node is located at approximately 0.2767 m from the bottom and 0.071 m from the side. In addition, there is a node that appears as a “ring” at the center of the model. This is probably due to the complex coupling between torsional and transverse modes of vibration.

5.2.6 Close Examination of the Blade Finite Element Solution

MSC.Patran 2001 r2a 29-Apr-03 21:38:44

Fringe: SC1:DEFAULT, A1:Mode 1 : Freq. = 47.685, Eig. = 2.26e+006, Translational-(NON-LAYERED) (MAG)

Deform: SC1:DEFAULT, A1:Mode 1 : Freq. = 47.685, Eigenvectors: Translational

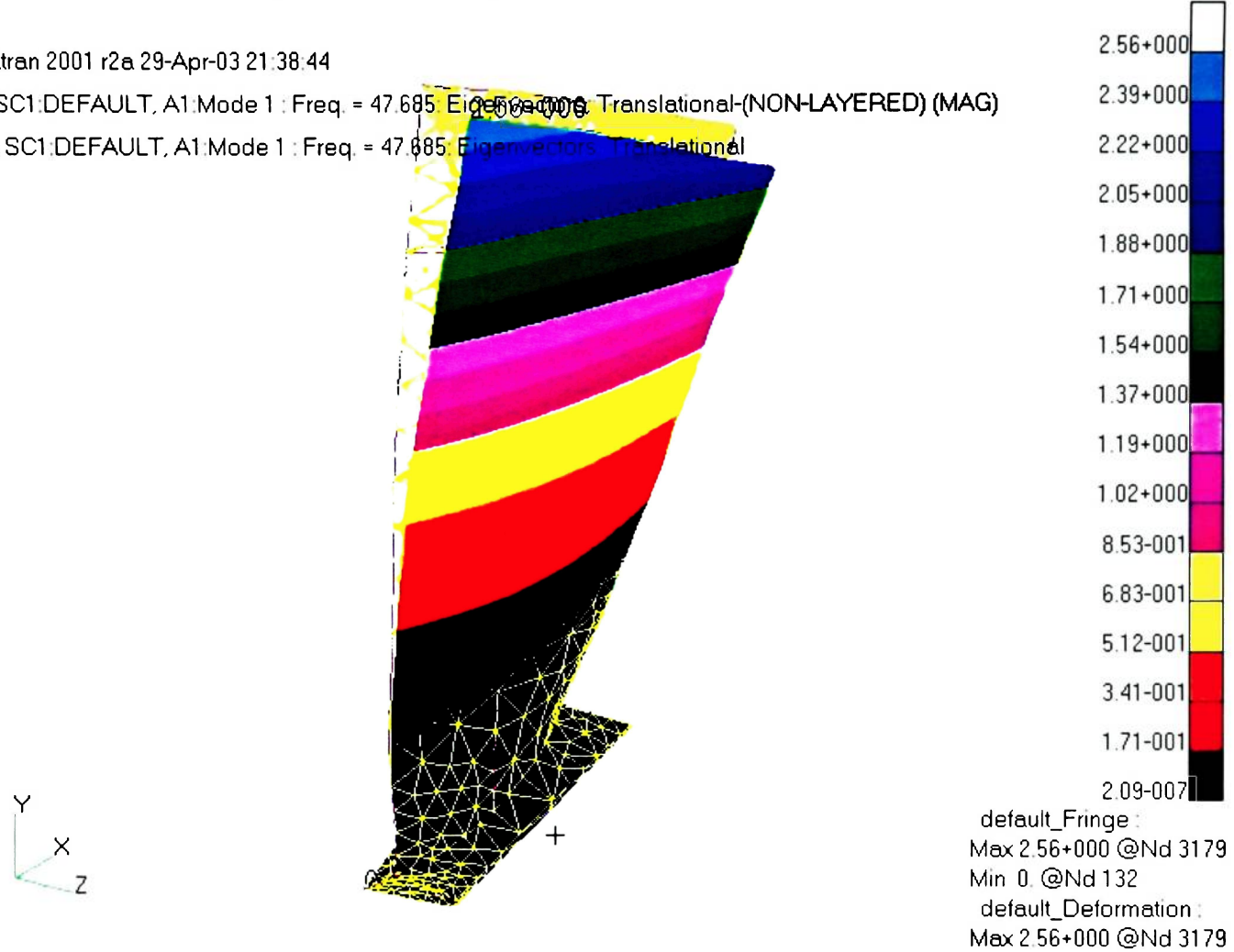


Figure 5.17: Mode 1 of the blade model

MSC.Patran 2001 r2a 29-Apr-03 21:53:24

Fringe: SC1:DEFAULT, A1:Mode 2 : Freq. = 227.98 Hz (NON-LAYERED) (MAG)

Deform: SC1:DEFAULT, A1:Mode 2 : Freq. = 227.98 Hz (NON-LAYERED) (MAG)

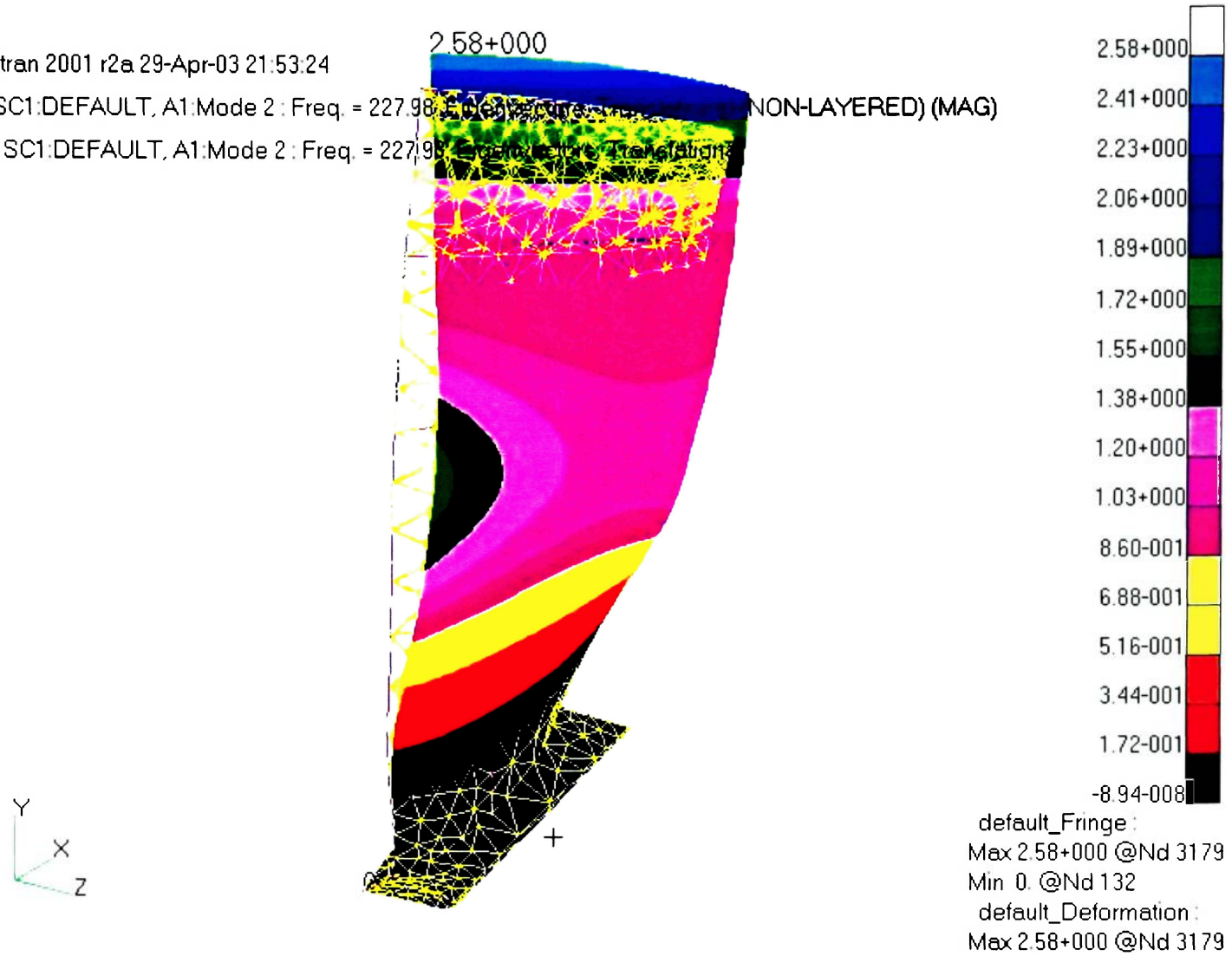


Figure 5.18: Mode 2 of the blade model

MSC.Patran 2001 r2a 29-Apr-03 21:54:49

Fringe: SC1:DEFAULT, A1:Mode 3 : Freq. = 296.87 Eigenvalue = 8.815e+007 Transitional-(NON-LAYERED) (MAG)

Deform: SC1:DEFAULT, A1:Mode 3 : Freq. = 296.87 Eigenvalue = 8.815e+007 Transitional

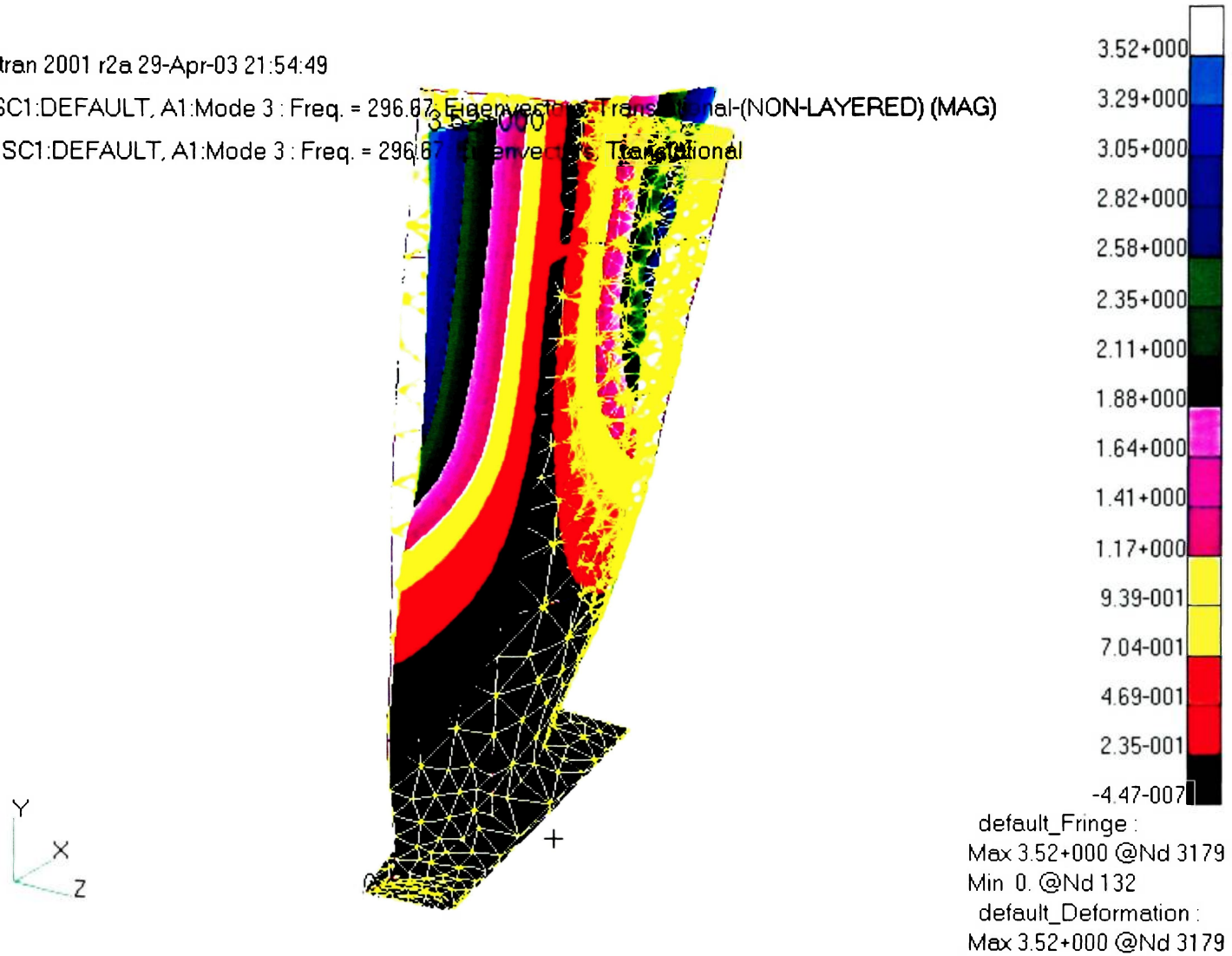


Figure 5.19: Mode 3 of the blade model

MSC.Patran 2001 r2a 29-Apr-03 21:56:31

Fringe: SC1:DEFAULT, A1:Mode 4: Freq. = 479.56 Eigenvectors, Translational-(NON-LAYERED) (MAG)

Deform: SC1:DEFAULT, A1:Mode 4: Freq. = 479.56 Eigenvectors, Translational

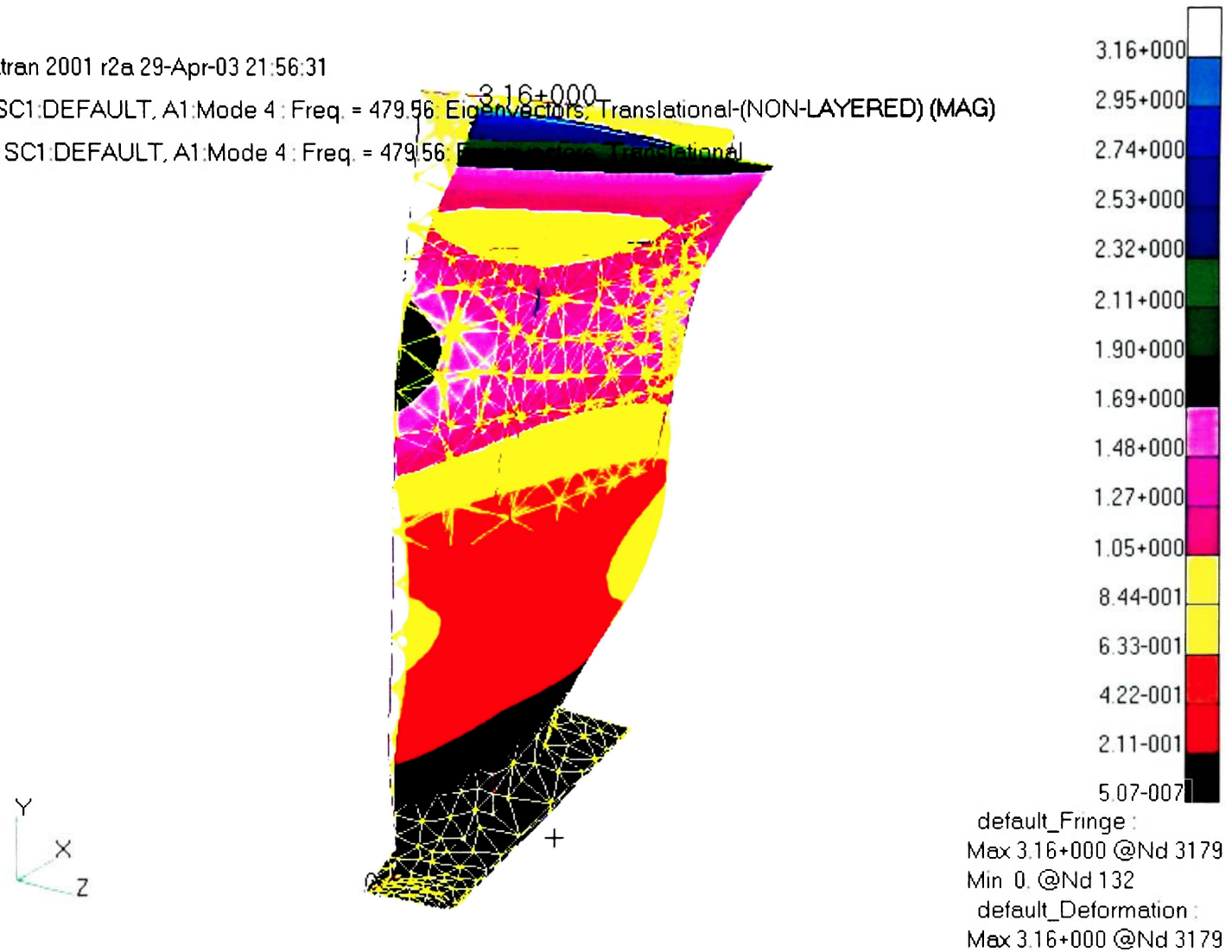


Figure 5.20: Mode 4 of the blade model

MSC.Patran 2001 r2a 29-Apr-03 21:58:12

Fringe: SC1:DEFAULT, A1:Mode 5 : Freq. = 983.18 Hz Eigenvectors: Translational-(NON-LAYERED) (MAG)

Deform: SC1:DEFAULT, A1:Mode 5 : Freq. = 983.18 Hz Eigenvectors: Translational

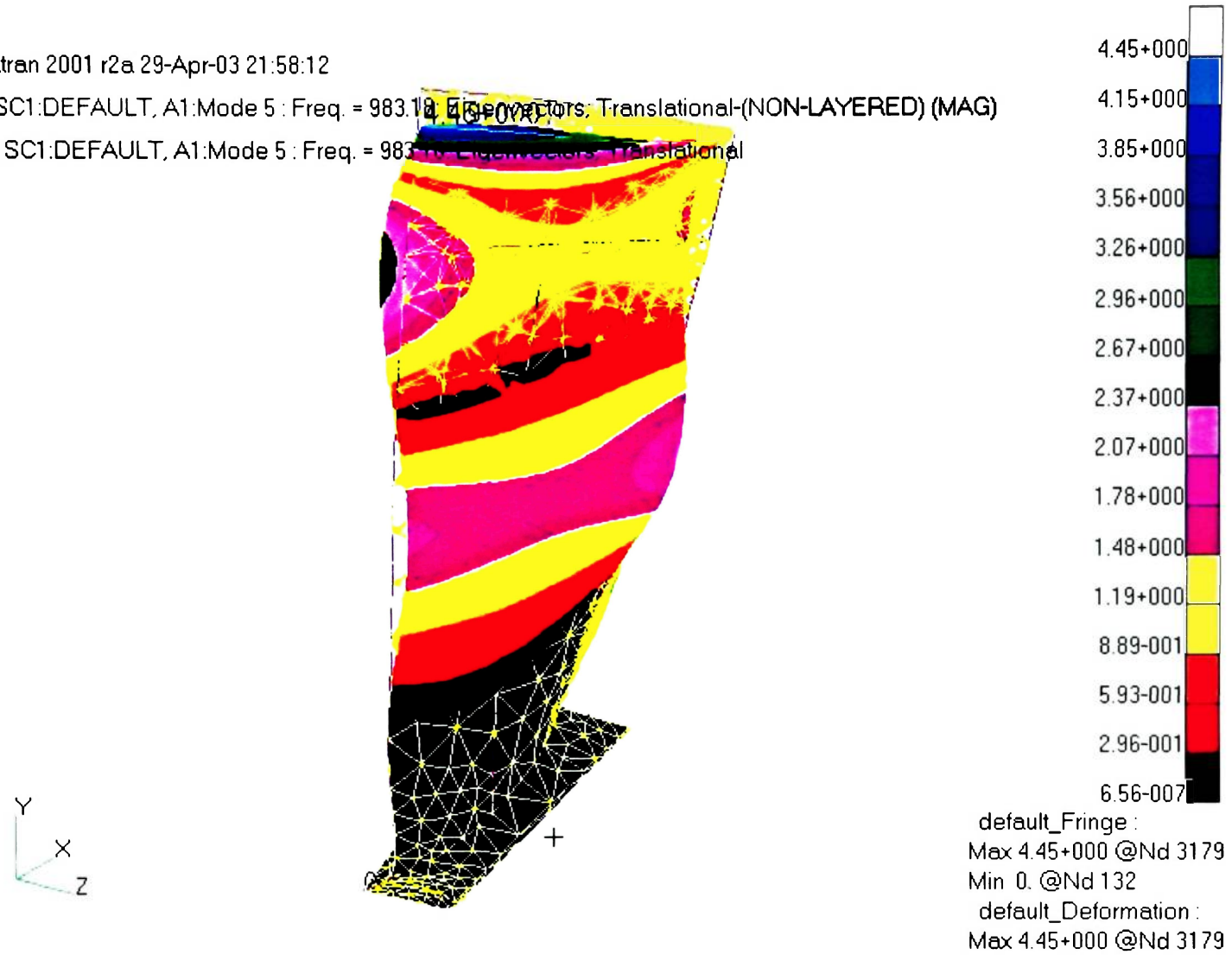


Figure 5.21: Mode 5 of the blade model

MSC.Patran 2001 r2a 29-Apr-03 21:59:26

Fringe: SC1:DEFAULT, A1:Mode 6 : Freq. = 1179.5 Eigenpairs: Translational (NON-LAYERED) (MAG)

Deform: SC1:DEFAULT, A1:Mode 6 : Freq. = 1179.5 Eigenpairs: Translational

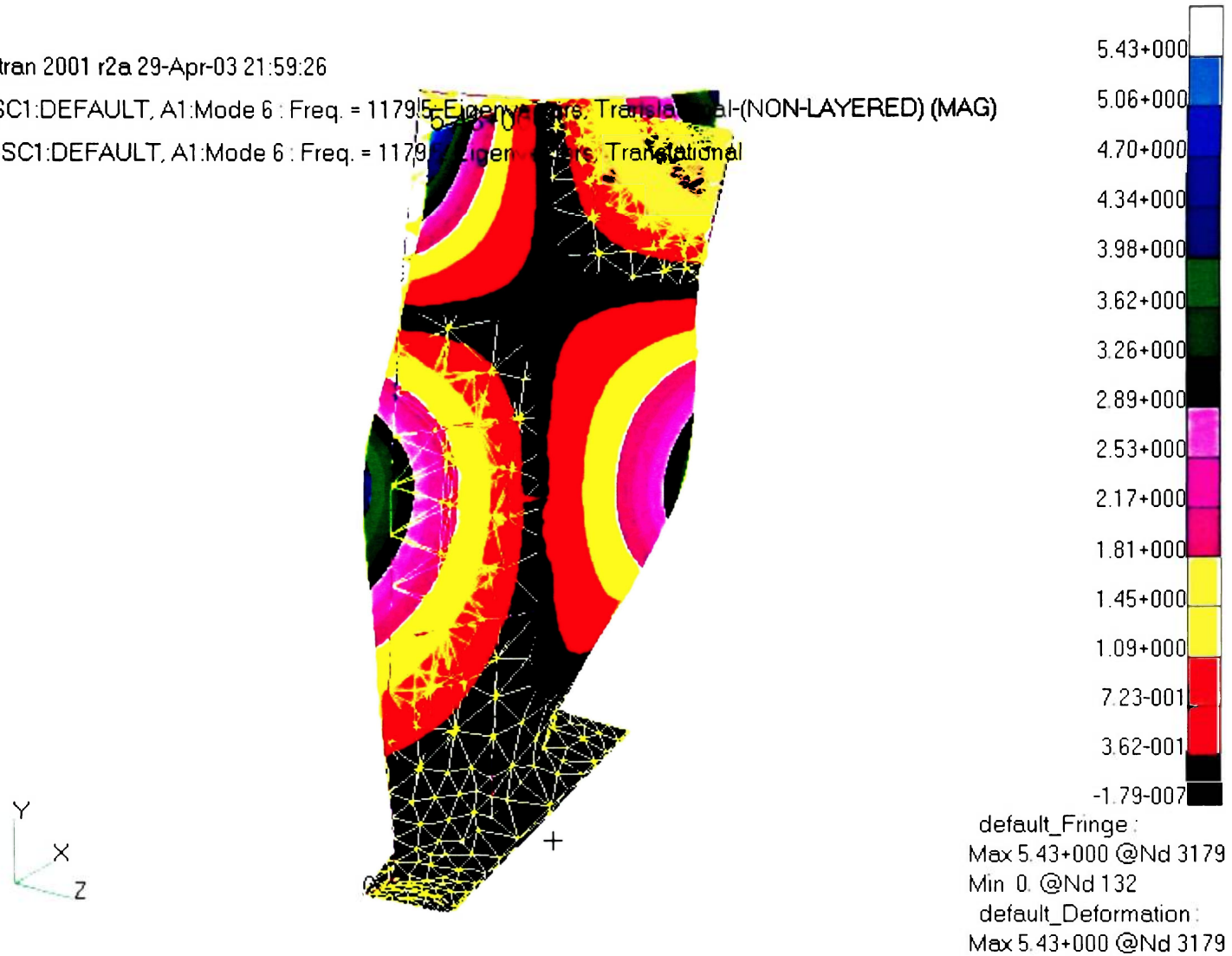


Figure 5.22: Mode 6 of the blade model

MSC.Patran 2001 r2a 29-Apr-03 22:00:58

Fringe: SC1:DEFAULT, A1:Mode 7 : Freq. = 1585.8; Eigenvectors: Translational-(NON-LAYERED) (MAG)

Deform: SC1:DEFAULT, A1:Mode 7 : Freq. = 1585.8; Eigenvectors: Translational

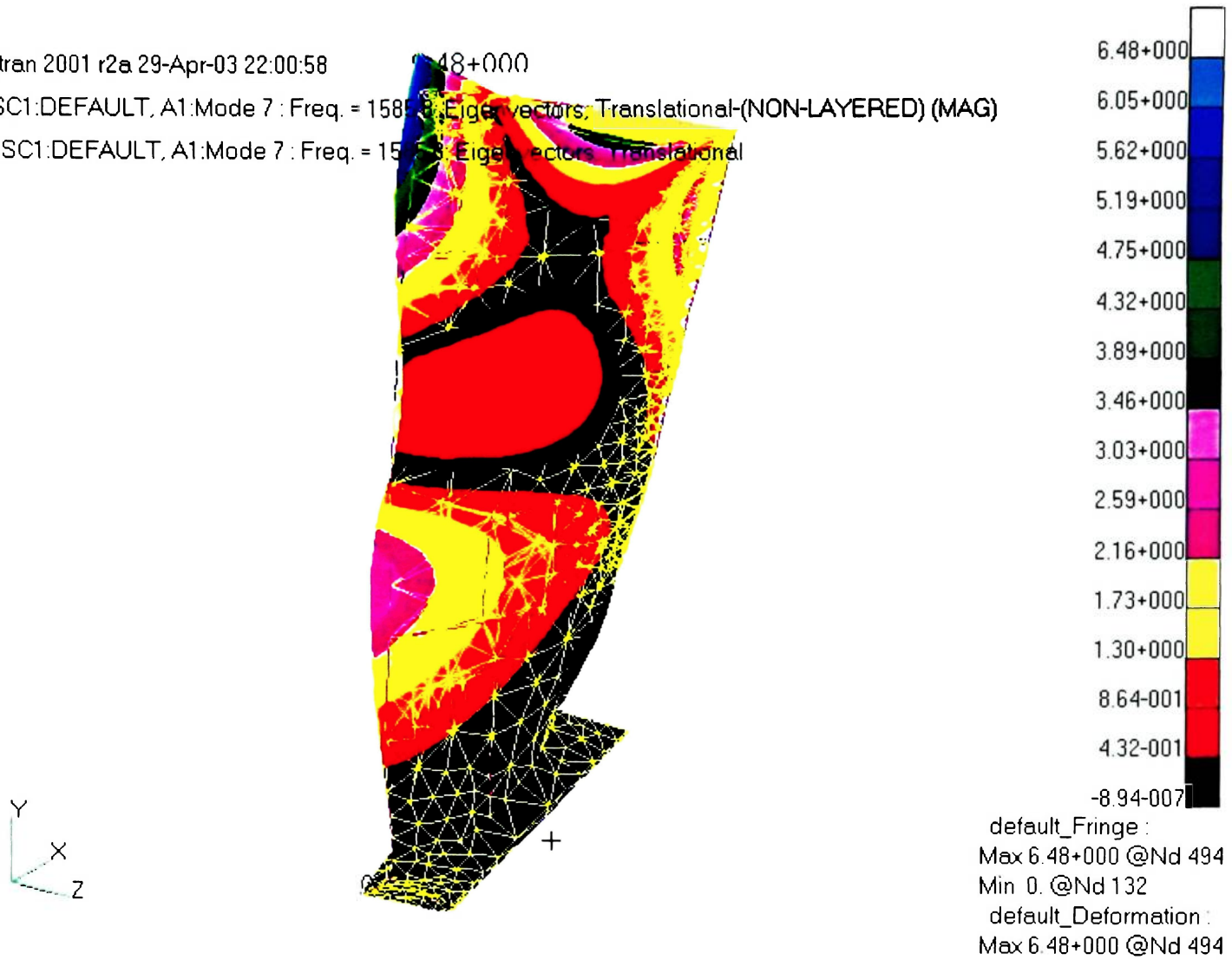


Figure 5.23: Mode 7 of the blade model

MSC.Patran 2001 r2a 29-Apr-03 22:03:17

Fringe: SC1:DEFAULT, A1:Mode 8 : Freq. = 1660.4, Eigenvector: Translational-(NON-LAYERED) (MAG)

Deform: SC1:DEFAULT, A1:Mode 8 : Freq. = 1660.4, Eigenvector: Translational

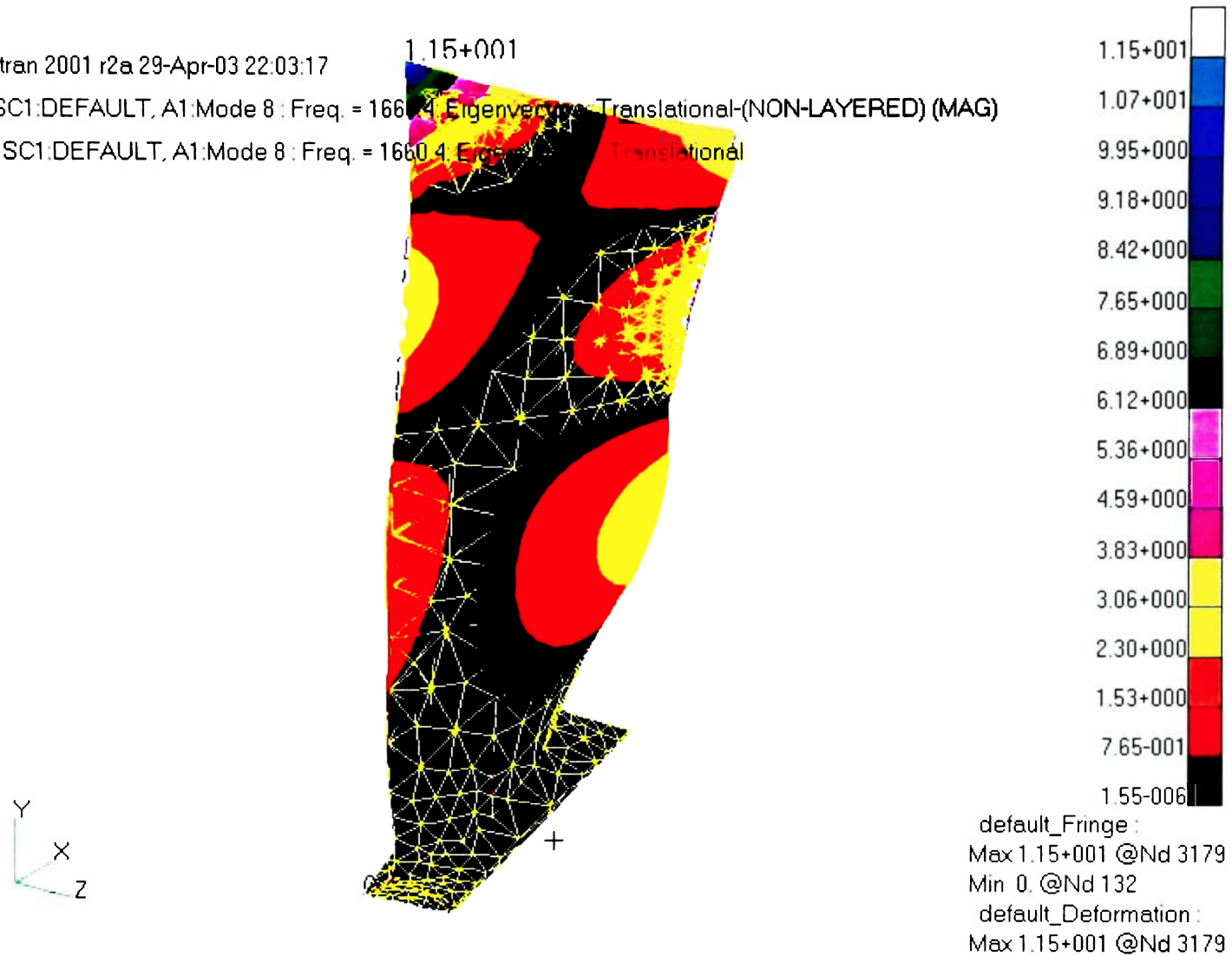


Figure 5.24: Mode 8 of the blade model

First mode of vibration represents the resonant vibration caused by an excitation at the first or fundamental natural frequency. Generally, the resonant vibration due to first several natural frequencies causes a highest amplitude displacement and prolonged blade operations near those ranges of frequencies should be avoided. The first natural frequency of the blade occurs at 47.685 hertz. Therefore, prolonged rotor operation near 2861 RPM should be avoided. As one may observe from Figure 5.17, the first vibration mode of the blade is dominantly transverse. The highest displacement occurs at the tip of the blade. In addition, the node does not exist for this mode of vibration due to the fact that the first transverse mode never intersects the zero displacement line. As mentioned previously, node is the location where the mode shape of vibration intersects the zero displacement line.

Second mode of vibration occurs when the blade is excited by a periodic force that has an oscillation frequency near the second natural frequency of the blade. As one may observe from Figure 5.18, the second vibration mode is dominantly transverse. In addition, the node occurs at approximately 0.3082 m to 0.3152 m from the bottom of the dovetail attachment. It should be noted that the slight torsional vibration is in effect and the node is not totally displacement-free, although it is the point of minimum displacement. For the analysis of the blade model, measurement is taken from the bottom of the dovetail attachment, not the blade bottom. Therefore, the length of the bottom attachment should be subtracted from the above node location when making comparisons with node locations obtained from other models. The second natural frequency of the blade is 227.98 hertz and the rotor speed of 13739 RPM can cause the resonant vibration.

Third mode of vibration is the result of an excitation at the third natural frequency. It is clearly visible from Figure 5.19 that the third vibration mode is dominantly torsional. In two-dimensional notation, this mode corresponds to $\omega_{1,2}$, which is the first anti-symmetric mode of the blade. Node location is at the center of the blade along its length and located approximately 0.0574 m to 0.0654 m from the blade front edge. The black line of the contour diagram represents the location where the displacement due to the vibration is not present. The third natural frequency of the blade is 296.67 hertz and prolonged excitation at 17920 RPM is not recommended.

Fourth mode of vibration occurs if the excitation frequency is at the fourth natural frequency of the blade. The fourth natural frequency of the blade is 479.56 hertz and rotational excitation near 28774 RPM should be avoided. In this mode, the blade has two nodes at approximately 0.3467 m to 0.3543 m and 0.1927 m to 0.2048 m from the bottom of the dovetail attachment. Although this mode characterized with dominantly transverse vibration, the small torsional displacement is still present at those node locations. Therefore, nodes are not completely displacement-free as in the case of second mode.

Fifth natural frequency for the blade is 983.18 hertz and the resonant vibration may occur at 58991 RPM, which is way above the operational speed of fan/compressor rotor. This mode is dominantly transverse and has two nodes. The first node occurs at approximately 0.3378 m to 0.3632 m from the bottom of dovetail. The second one occurs at approximately 0.2611 m to 0.2803 m and can be seen clearly in Figure 5.21 as a black spot.

Sixth mode of vibration occurs at 1179.5 hertz. The diagram clearly depicts the node that represents $\omega_{2,2}$ of two-dimensional vibration. It also shows a coupling between

torsional and transverse vibration. The transverse node occurs at approximately 0.3034 m to 0.3112 m from the bottom of dovetail. The torsional node occurs at the center of the blade along its length and located at approximately 0.0654 m to 0.0703 m for the blade front edge.

Seventh natural frequency of vibration for the blade is 1585.8 hertz and it is high enough that vibration due to this frequency is not a concern for the normal blade operation. This mode exhibits both torsional and transverse vibration and its natural frequency corresponds to $\omega_{3,2}$ in two-dimensional notation. Mode shape is somewhat complex and it is difficult to describe them in words. Therefore, the diagram in Figure 5.23 should be consulted to locate the approximate position of nodes.

Eighth mode of vibration of the blade occurs at 1660.4 hertz. This mode is a combination of torsional and transverse vibration. As one may observe, several nodes are available and they can be seen clearly in Figure 5.24 as black lines.

Chapter 6

Conclusion

The analytical results were obtained using Bernoulli-Euler, Timoshenko, Rayleigh, Rayleigh-Ritz, two-dimensional plate, Timoshenko beam methods. In the previous chapter, the analytical results were compared with finite element solutions. The analytical results clearly revealed the validity of finite element solutions. It was observed that the beam models (Bernoulli-Euler beam) and two-dimensional plate model compared well with the finite element solution of the blade model. The Rayleigh and Rayleigh-Ritz methods did not correlate well with the actual blade model due to the fact that the thickness of the real blade tapers exponentially, not linearly. However, when the Rayleigh's method was compared with the finite element solution of tapered beam (not the actual blade model), the valid correlation was established. The solution from Rayleigh-Ritz method did not compare well with the tapered model solution either. As mentioned previously, the error of Rayleigh-Ritz solution is the result of the insufficient terms used in the mode shape function.

The vibration characteristics of a straight plate determined by the finite element analysis closely resembles the plate analytical solution. As one can observe from Table 6.10, vibration types and natural frequencies of plate finite element solution is extremely similar to the analytical reference, except for the chordwise vibration mode that could not be depicted by any analytical methods. This close resemblance is due to the fact that the plate analytical solution was obtained using the analytical model similar to the plate finite element model (in fact, almost identical).

The blade model consists of twisted geometric figure, unlike other finite element models (straight plate and tapered solid). Due to this difference in the geometric figure, the blade finite element solution differs substantially from other finite element solutions for some vibration modes. Nevertheless, the blade model shares the similar vibration characteristics with the analytical models and other finite element models for majority of the cases, as shown in the previous chapter. Therefore, it is concluded that the blade finite element solution is valid and accurate. The main objective of this thesis was successfully accomplished.

Chapter 7

Recommendation

7.1 Effect of Blade and Rotor Joints

In this thesis, the constraint condition of the finite element model at the root of the blade is considered as a connection rigidly fixed onto the “wall”. In fact, there are other considerations that could be made to improve the finite element solution. Generally, compressor/fan blade is attached to a rotor disk by joints that the “dovetail” of a blade is slid into the “Christmas tree” slots of the rotor disk. Although the joints are tightly fixed together when the engine is not in the operation, they may not be as rigid when the engine is in the operation [7]. In other words, the coupling stiffness between blades and the rotor in service may differ substantially from the rigidly fixed condition. Therefore, it may be more proper to assume that blades are “flexibly” fixed to a rotor disk. The research on the flexibly fixed constraint for blade/rotor joints was conducted by Jian F Hou [7]. In order to simulate the flexibly fixed joints, Hou combined a rotor model and a blade model into a single finite element model. Consequently, the interaction between blades and the rotor is similar to the behavior of sliding joints with certain stiffness. This system interaction altered the problem nonlinear in nature. The research revealed that natural frequencies of the system (blade and rotor) are lower than that of the blade alone by several percent, depending on the mode of vibration. Unfortunately, at the time of this writing, the university did not possess finite element program (solver) that is capable of non-linear dynamics analysis in this degree. The recommendation should be made here for the future research that nonlinear dynamics behaviors results from this flexibly fixed

joint may be important and should be considered instead of assuming the rigidly fixed constraint at the blade bottom.

7.2 Gap Contacts between Blade Attachments

Previously, the assumption was made that two protruding figures on a blade can be considered as a single concentrated mass. In the normal operation of the engine, those protruding figures actually serve as attachments between adjacent blades. Since those attachments are not rigidly fixed to one another, the finite element model to represent this condition must not be a fixed constraint. In addition, each attachment is separated from the adjacent one by an extremely small gap. Two adjacent attachments are bumping and sliding on each other during the normal engine operation. Therefore, the best representation of the interaction between attachments is the combination of gap contacts and sliding lines. Although gap contacts and sliding lines can be easily modeled using MSC.PATRAN, the dynamics problem involving those movable constraints are nonlinear in nature and not solvable by standard MSC.NASTRAN (requires special option) [9]. Thus, the problem of this nature is considered beyond the scope of this research project.

7.3 Forced Vibration Analysis and Computational Fluid Dynamics (CFD)

The purpose of normal mode analysis performed in this thesis is to determine natural frequencies and mode shapes of the compressor/fan blade. Using the natural frequencies, the analysis involving the forced vibration can be performed. The forced vibration analysis can be subdivided into two categories, frequency response analysis and transient response analysis. In frequency response analysis, the excitation is explicitly defined in the frequency domain and structural responses to the steady-state oscillatory

excitation are computed. The transient response analysis is utilized when the structural response to the time-varying excitation is desired.

In order to perform a forced vibration analysis, nature of the excitation force on the blade surface must be known. The most reliable and probably the only method to accurately determine the aerodynamic force is the computational fluid dynamics (CFD). The force intensity, location, and any types of information regarding the aerodynamic pressure being applied to the blade surface can be found using CFD. One of the most popular CFD solver available today is FLUENT and the meshing program, GAMBIT. The same CAD model (CATIA model) used for PATRAN can also be used by GAMBIT to mesh the external space around the blade. Then, FLUENT solver can solve the fluid mechanics problem using this external mesh. Since the University has both FLUENT and GAMBIT programs, it is probably not a difficult task to perform a CFD on the blade model. Therefore, the recommendation should be made here that CFD, instead of classical aerodynamics, should be utilized to determined aerodynamic forces.

7.4 Aerodynamic and Structural Damping

This research project was performed with an assumption that there are no damping effects present in the blade vibration. Although this is a good assumption for the free vibration analysis, it may not be sufficient for forced vibration analysis. Two major types of damping effects for a rotating blade are the aerodynamic damping and the structural damping. Aerodynamic damping results from the interaction between aerodynamic forces and the blade motion. Therefore, it can be determined by theory of aeroelasticity. Structural damping is the inherent tendency of the blade to reduce the intensity of vibration by itself. These damping effects may hold importance in the forced

vibration analysis. Therefore, inclusion of aerodynamic and structural damping effects can be considered as the future work.

References

- [1] Rao, S. S., "Mechanical Vibration," 3rd edition, Addison-Wesley, 1995
- [2] Cook, R. D., Malkus, D. S., Plesha, M. E., and Witt, R. J., "Concept and Applications of Finite Element Analysis," 4th edition, John Wiley & Sons, 2002
- [3] Ayre, R. S., and Jacobsen L. S., "Engineering Vibrations with Applications to Structures and Machinery," McGraw-Hill, 1958
- [4] McDougal, W. G., Ross, C. A., and Tedesco, J. W., "Structural Dynamics: Theory and Applications," Addison-Wesley, 1999
- [5] Yang, T. Y., "Finite Element Structural Analysis," Prentice-Hall, 1986
- [6] Kruse, M., and Pierre, C., "Dynamic Response of an Industrial Turbomachinery Rotor," AIAA paper 96-2820, July 1996
- [7] Hou, J. F., "Blade Vibrations Coupled with Disks," AIAA paper 2002-1668, April 2002
- [8] MSC Software, "MSC.visualNastran: User's Guide," 2001
- [9] MSC Software, "Dynamic Analysis using MSC.Nastran for Windows: Work Book," 1999
- [10] Craig, R. R., "Structural Dynamics: An Introduction to Computer Methods," John Wiley & Sons, 1981
- [11] Rosenbaum, R., Scanlan, R. H., "Introduction to the Study of Aircraft Vibration and Flutter," Macmillan, 1951
- [12] Gorman, D. J., "Free Vibration Analysis of Rectangular Plates," Elsevier, 1982
- [13] Chopra, A. K., "Dynamics of Structures: Theory and Application to Earthquake Engineering," Prentice-Hall, 1995
- [14] MSC Software, "Dynamic Analysis using MSC.Nastran for Windows: Course Notes," 1999
- [15] MSC Software, "MSC.Nastran for Windows: Analysis Example Manual," 1998
- [16] Fleeter, S., Zhou C., Houstis E., and Rice J., "Fatigue Life Prediction of Turbomachine Blading," Research paper, Purdue University, 2000

Appendix

Eigenvalue Extraction Methods

There are several methods of real eigenvalue extraction that can be presented here. These methods are numerical approaches to solving for natural frequencies and modes shapes. While most of the methods can be applied to all problems, the choice is often made based on the efficiency of the solution process [14].

The methods of eigenvalue extraction belong to one or both of the following two groups.

- Transformation methods
- Tracking methods

In transformation method, the eigenvalue equation is first transformed into a special form from which eigenvalue may easily be extracted. In tracking method, the eigenvalues are extracted one at a time using an iterative procedure.

The most popular and recommended eigenvalue extraction method is the Lanczos method. The Lanczos method combines the best characteristics of both the tracking and transformation methods. For most finite element analysis, the Lanczos method is the best method to use for its obvious advantages. Other popular eigenvalue extraction methods are shown below.

- Transformation methods
 - Lanczos method
 - Givens method

- Householder method
- Modified Givens method
- Modified Householder method
- Tracking method
 - Inverse power method
 - Sturm modified inverse method

A1 Lanczos Method

The Lanczos method overcomes the limitations and combines the best features of the other eigenvalue extraction methods. It requires that the mass matrix to be positive semi-definite and the stiffness matrix to be symmetric. Like the transformation methods, it does not miss any roots, but has the efficiency of the tracking methods, because it only makes the calculations necessary to find the desired roots. This method computes accurate eigenvalues and eigenvectors. Over past few decades, its performance has been continually enhanced since its introduction and giving it a great advantage over other methods. The Lanczos method is the preferred method for most medium to large size problem, since it has a performance advantage over other methods. Therefore, Lanczos is the choice of computation method for this research project.

A2 Givens and Householder Method

The Givens and Householder modal extraction methods require a positive definite mass matrix (all DOF must have mass). There is no restriction on the stiffness matrix except that it must be symmetric. These matrices always result in real or positive eigenvalues. The Givens and Householder methods are the most efficient method for

small problems and problems with dense matrices when large portions of the eigenvectors are needed. These methods find all of the eigenvalues and as many eigenvectors as desired.

The Givens and Householder methods fail if the mass matrix is not positive definite. To minimize this problem, degree-of-freedom with null columns are removed by the application of static condensation. The static condensation process may not be able to remove all possible causes of mass matrix singularity, but it greatly improves the reliability of the Givens and Householder methods.

A3 Modified Givens and Modified Householder Methods

The modified Givens and modified Householder methods are similar to their original methods with the exception that the mass matrix can be singular. Although the mass matrix is not required to be nonsingular in the modified methods, a singular mass matrix can produce one or more infinite eigenvalues. Due to round-off error, these infinite eigenvalues may appear in the output as very large positive or negative eigenvalues. To reduce such irrelevant results, degree-of-freedom with null masses are eliminated by static condensation.

A4 Inverse Power Method

The inverse power method is a tracking method since the lowest eigenvalue and eigenvector in the desired range are found first. Then, higher roots are found by an iterative procedure. The inverse power method is unpopular method since it can miss modes. The Strum modified inverse power method presented next is a more reliable tracking method.

A5 Sturm Modified Inverse Power Method

This method is similar to the inverse power method except that it uses Sturm sequence logic to ensure that all modes are found. The Sturm sequence check determines the number of eigenvalues lower than a trial eigenvalue, and then finds all of the eigenvalues lower than this trial eigenvalue until all modes in the desired range are computed. This process helps to ensure that modes are not missed. The Sturm modified inverse power method is useful for an analysis in which only the lowest few modes are needed. This method is also useful as a backup method to verify the accuracy of other methods.